

20 JUNI 1968

TECHNISCHE HOOGESCHOOL DELFT
VUEGTUIGBOUWKUNDE
BIBLIOTHEEK

NATIONAL RESEARCH COUNCIL OF CANADA

AERONAUTICAL REPORT
LR-492

VIBRATION MODES AND RANDOM RESPONSE OF A
MULTI-BAY PANEL SYSTEM USING FINITE ELEMENTS

BY

GARRY M. LINDBERG AND MERVYN D. OLSON
NATIONAL AERONAUTICAL ESTABLISHMENT

OTTAWA
DECEMBER 1967

NCR NO. 10001



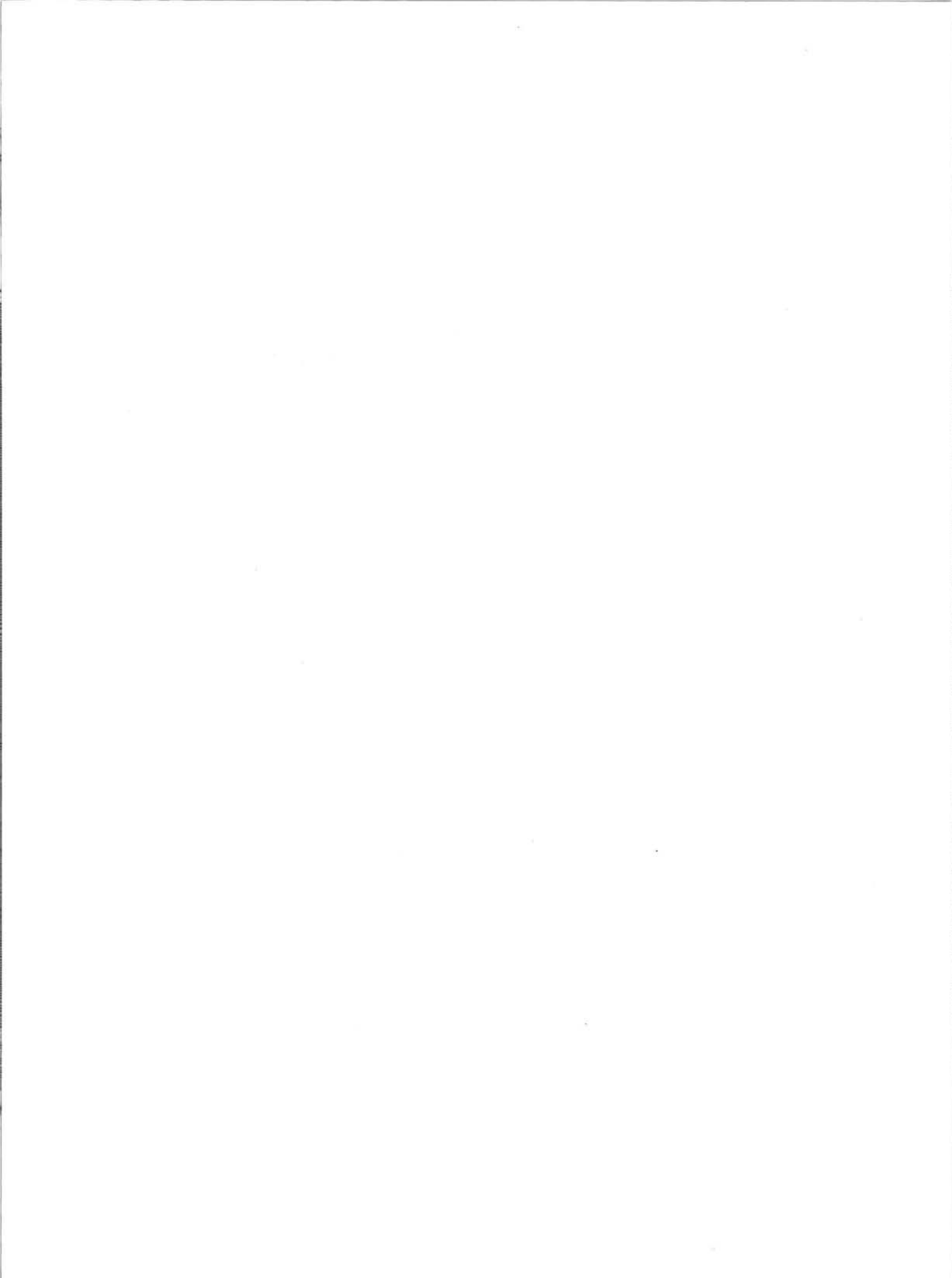
VIBRATION MODES AND RANDOM RESPONSE OF A
MULTI-BAY PANEL SYSTEM USING FINITE ELEMENTS

BY

GARRY M. LINDBERG and MERVYN D. OLSON

A.H. Hall, Head
Structures and Materials Section

F.R. Thurston
Director



SUMMARY

A finite element approach to the dynamic analysis of continuous skin-stringer panels is presented. The method is illustrated in the calculation of vibration modes and random response of a five-bay stringer-stiffened panel with all outer edges clamped. The panel skin is represented by finite plate elements and the stringers, which are assumed infinitely stiff in bending, are represented by beam torsional elements.

Results are presented for the first 35 panel vibration modes. These modes occur in distinct groups with five similar modes in each, the number five corresponding to the number of panel bays. The response of the panel to plane wave propagation of acoustic noise (propagating normal to the stringers) is also calculated. The resulting response power spectral densities were found to be fundamentally different from those associated with single span panels. These power spectra did not have widely separated peaks, but rather the peaks tended to be squeezed into groups corresponding to the groupings of natural frequencies for the panel.

TABLE OF CONTENTS

	Page
SUMMARY	(iii)
TABLES	(iv)
ILLUSTRATIONS	(v)
APPENDIX	(v)
SYMBOLS	(vi)
1.0 INTRODUCTION	1
2.0 THEORETICAL FORMULATION	2
2.1 Finite Plate Elements	3
2.2 Torsional Element	4
2.3 Vibration Modes and Random Response	6
3.0 EXAMPLE APPLICATION	8
3.1 Vibration Modes	10
3.2 Random Response	12
4.0 CONCLUDING REMARKS	16
5.0 REFERENCES	17

TABLES

Table	Page
I Stiffness Matrix for Finite Plate Element	19
II Mass Matrix for Finite Plate Element	20
III Five Bay Panel Vibration Frequencies	21
IV Effect of Stringers on Panel Frequencies	22

ILLUSTRATIONS

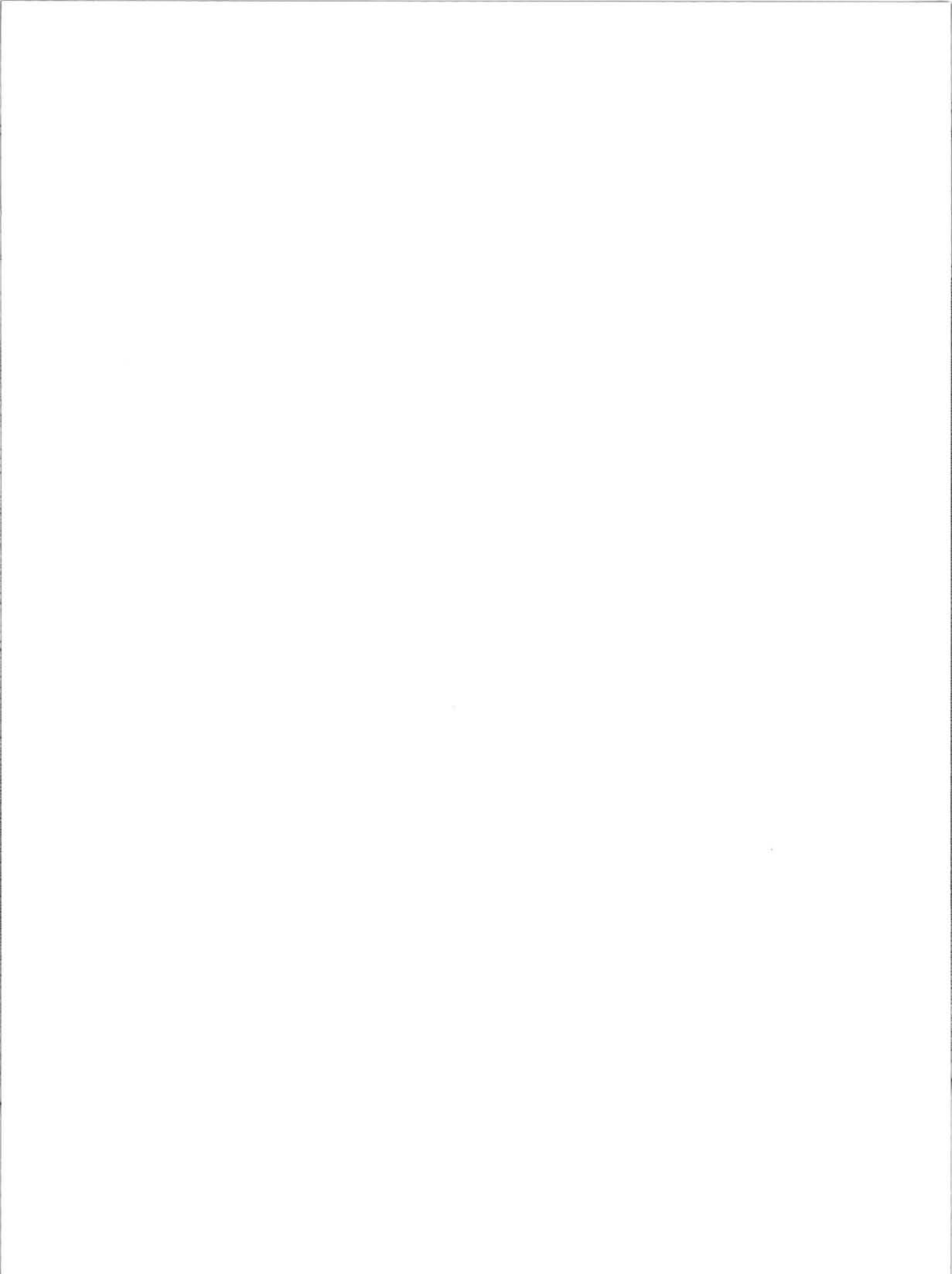
Figure		Page
1	Identically Constructed Panels	23
2	Five-Bay Stringer-Stiffened Panel	24
3	Plate Element	25
4	Torsional Beam Element	26
5	Finite Element Representations for Five-Bay Panel	27
6 - 23	Five-Bay Panel Vibration Modes	28-45
24	PSD for w_1 On Five-Bay Panel	46
25	PSD for w_3 On Five-Bay Panel	47
26	PSD for w_7 On Five-Bay Panel	48
27	PSD for w_9 On Five-Bay Panel	49
28	PSD for w_{13} On Five-Bay Panel	50
29	PSD for w_{15} On Five-Bay Panel	51
30	PSD for w_{19} On Five-Bay Panel	52
31	PSD for w_{21} On Five-Bay Panel	53
32	PSD for w_{25} On Five-Bay Panel	54
33	PSD for w_{27} On Five-Bay Panel	55
34	PSD for ψ_{x27} On Five-Bay Panel	56
35	PSD for ψ_{y27} On Five-Bay Panel	57
36	Longitudinal Distribution of RMS Panel Response	58
37	Lateral Distributions of RMS Panel Response	59
APPENDIX A		
	Derivation of Stringer Torsional Element	61

SYMBOLS

Symbol	Definition
$a_0 - a_{11}$	Arbitrary constants, eq. (1)
a, b	Length and width of plate element, Fig. 3
B	Complex influence matrix = $B_R + iB_I$, eq. (11)
c	Acoustic propagation speed = 1140 fps
C_w	Warping constant
d, e	Height and width of stringer cross section, Fig. 2
D	Plate bending rigidity = $E h^3 / 12(1 - \nu^2)$
E	Young's modulus
$\vec{f}(t)$	Transverse load vector, eq. (9)
$\vec{F}(\omega)$	Fourier transform of load vector, eq. (10)
g	Structural damping parameter, eq. (8)
h	Plate or panel thickness
I	Moment of inertia for stringer, Appendix A
K	Stiffness Matrix, eq. (7)
l	Length of stringer element, Appendix A
L	Overall length of five-bay panel
M	Mass matrix, eq. (7)
$M_{xi}, M_{yi} (i=1, 4)$	Corner moments on plate element, Fig. 3
$\overline{p_0^2}$	Mean square acoustic pressure
P	Damping matrix, eq. (8)
$S_{Fjk}(\omega)$	Cross-spectral density for load vector, eq. (14)
$S_{xii}(\omega)$	Power spectral density for displacement component x_i

SYMBOLS (Cont'd)

Symbol	Definition
$S_w(\omega)$	Power spectral density for panel displacement w
$S_\psi(\omega)$	Power spectral density for panel slope ψ
T_1, T_2	End torques on torsional beam element, Appendix A
$V_i (i=1, 4)$	Corner shears on plate element, Fig. 3
w	Panel displacement
$w_i (i=1, 4)$	Corner displacements on plate element, Fig. 3
W	Width of five-bay panel
$\vec{x}(t)$	Panel displacement vector
$\vec{X}(\omega)$	Fourier transform of displacement vector $\vec{x}(t)$
x, y	Panel and plate element co-ordinates, Fig. 2 and 3
α	Frequency parameter = $\mu \omega^2 a^4 / 1680 D$, eq. (10)
θ_1, θ_2	End rotations of torsional beam element, Appendix A
λ	Eigenvalue
μ	Panel mass per unit area = ρh
ν	Poisson's ratio
ρ	Panel material density
$\psi_{xi}, \psi_{yi} (i=1, 4)$	Corner slopes of plate element, Fig. 3
ω	Circular frequency
ω_c	Cut-Off frequency for white acoustic noise



VIBRATION MODES AND RANDOM RESPONSE OF A MULTI-BAY
PANEL SYSTEM USING FINITE ELEMENTS

1.0 INTRODUCTION

Almost all aerospace structures incorporate some sort of panel-rib-stringer configuration. One of the most common is that in which a thin continuous panel is attached to closely spaced, flexible stringers and relatively stiffer and wider spaced ribs running at right angles to the stringers. The number and complexity of possible vibration modes in such a configuration increase rapidly with the number of bays. As a result, the work required to analyze the random response of this kind of structure, using the customary modal methods, soon becomes prohibitive. Furthermore, the modal frequencies are not widely separated, but rather become squeezed together into distinct bands, the number of frequencies in each band usually being equal to the number of panel bays. This fact implies that the correlations between different modes will no longer be negligible, thereby further increasing the complexity of the modal analysis.

One alternate approach to these problems is the method of transfer matrices; this has been successfully developed by Lin (Ref. 1) and Mercer and Leavey (Ref. 2). This method is somewhat limited, however, in that it is based on the assumption that the panel is simply supported along the ribs.

Another approach, which can account for other boundary conditions (e.g. clamped edges) along the ribs, is to use finite element techniques. This method is developed and illustrated with an example application in this Report.

The analysis for a five-bay, stringer-stiffened panel with all outer edges clamped is presented in detail. The stringers are considered to be infinitely stiff in bending but to have finite torsional stiffness and rotational inertia. Finite plate elements are used to represent the panel. These are the well-known twelve degree of freedom models derived from virtual work principles. Calculations of the vibration frequencies and mode shapes for the

panel assembly are carried out using a 3×3 and a 4×4 gridwork of elements for each bay. An ad hoc approximation for the effective stringer torsional stiffness and rotational inertia is used to derive corrections to the system stiffness and mass matrices, respectively.

The random response of this five-bay panel system is also presented for the particular type of excitation known as plane wave propagation (propagating normal to the stringers) of clipped white acoustic noise. The calculations are carried out for the 3×3 element grid per bay representation, with the excitation approximated by concentrated shear forces acting at the finite element corner junctions. The resulting dynamic system is analyzed by a generalized harmonic method, and the power spectral density for each degree of freedom is calculated for particular frequencies. These power spectral densities are then integrated numerically over all frequencies to obtain the mean square response of the panel system.

2.0 THEORETICAL FORMULATION

A typical configuration used in many aerospace structures is depicted in Figure 1. The design incorporates a thin, continuous panel either bonded or riveted to a framework of ribs and stringers running at right angles to each other. The example illustrated is especially simple in that all panels are identically constructed.

The analysis of the complete structure shown in Figure 1 is beyond present day capabilities and, hence, some simplifying approximations must be introduced. It has been found in practice that the stringers are generally much more flexible than the ribs, and are usually spaced much closer to each other. These conditions suggest the now well-known approximation of neglecting all interactions between panels across the ribs. This leaves only the problem of analyzing a single row of panels and stringers, as depicted in Figure 2.

Previous transfer matrix approaches to this problem (Ref. 1 and 2)

have employed the assumption of simply supported boundary conditions at the ribs. Unfortunately, this assumption is in direct conflict with the assumption of no interaction between panels across the ribs. It is clear that it would be more consistent to assume clamped boundary conditions at the ribs. However, the transfer matrix technique is not applicable in the case of clamped boundaries because the spatial dependence of the panel deflection is no longer separable.

2.1 Finite Plate Elements

In the case of clamped boundaries an exact solution is unattainable, and approximate techniques must be employed. The approach taken here, which is proving most efficient, is the use of finite plate elements. These are the well-known twelve degree of freedom models derived from virtual work principles. The derivation of the stiffness and mass matrices for these elements is well documented (Ref. 3 and 4) and need only be described briefly.

Consider the plate element shown in Figure 3. The deflection of any point on this element may be expressed as a finite series of polynomials in x and y as

$$\begin{aligned} w(x,y) = & a_0 + a_1 x + a_2 y + a_3 xy + a_4 x^2 + a_5 y^2 \\ & + a_6 x^2 y + a_7 xy^2 + a_8 x^3 + a_9 y^3 + a_{10} x^3 y + a_{11} xy^3 \end{aligned} \quad (1)$$

Note that this equation is the general solution of the biharmonic plate equation

$$D \nabla^4 w = 0 \quad (2)$$

The arbitrary constants in equation (1) are determined as functions of the twelve corner displacements ψ_{xi} , ψ_{yi} , w_i ; ($i = 1$ to 4) for the element. Then substitution back into equation (1) yields an equation relating the displacement anywhere on the element to the displacements of the four corner points. Differentiating this equation and substituting into the strain-displacement relations from plate

theory yields the element strains, and finally, substituting these strains into Hooke's Law yields the element stresses.

The plate element has external corner forces M_{xi} , M_{yi} , V_i ; ($i = 1$ to 4) (Fig. 3) acting on it that must be in equilibrium with the internal stresses. The stiffness matrix relating these corner forces with the corner displacements is obtained from the principle of virtual work. That is, the system is subjected to a set of compatible virtual displacements, and the external virtual work done by the external forces is equated to the internal virtual work done by the stresses. This equation yields the stiffness matrix shown in Table I.

The distributed mass matrix is found similarly by equating the external virtual work done by the external D'Alembert forces to the internal virtual work done by the internal D'Alembert forces. The resulting mass matrix is shown in Table II, where the asterisks designate D'Alembert forces.

2.2 Torsional Element

As mentioned in the Introduction, for the problem of interest herein the stringers are considered infinitely rigid in bending but have finite torsional stiffness and rotational inertia. Hence, an approximation for this stiffness and inertia that is compatible with the finite plate element representations is required.

A consistent lumped parameter representation for the simple torsional beam element shown in Figure 4 as derived in Appendix A is

$$\begin{bmatrix} T_1 \\ T_2 \end{bmatrix} = \frac{GJ}{\ell} \begin{bmatrix} 1 & -1 \\ -1 & 1 \end{bmatrix} \begin{bmatrix} \theta_1 \\ \theta_2 \end{bmatrix} - \frac{\omega^2 I \ell}{6} \begin{bmatrix} 2 & 1 \\ 1 & 2 \end{bmatrix} \begin{bmatrix} \theta_1 \\ \theta_2 \end{bmatrix} \quad (3)$$

where T_1 and T_2 are the externally applied torques, and θ_1 and θ_2 are the

resulting rotations at the two ends of the element. The equivalent lumped parameter representation for a plate element with a stringer attached to one edge may now be obtained by suitably incorporating the results of equation (3) into the stiffness and mass matrices for the plate.

However, the simple beam element used as the basis for equation (3) is not a good approximation for the type of stringers depicted in Figure 2 because it neglects the effect of cross-sectional warping. This deficiency may be corrected by replacing the torsional stiffness factor GJ in equation (3) by an effective stiffness factor $(GJ)_e$ that includes some warping effect. The equation governing the motion of a stringer attached to a panel (eq. (7-129) in Ref. 1) is

$$E C_w \frac{\partial^5 w}{\partial x^4 \partial y} - GJ \frac{\partial^3 w}{\partial x^2 \partial y} + \text{Inertia terms} = M_r - M_l \quad (4)$$

where C_w is the warping constant with respect to the shear centre, and M_r and M_l are the moments transmitted from the skin panel on the right and left, respectively, of the stringer considered (see Fig. 2 for co-ordinate system). In order to obtain an estimate of the effect of warping, it is assumed that the panel deflection has n half waves in the y direction, hence w is approximately proportional to $\sin \frac{n\pi y}{W}$. Equation (4) may then be put in the form

$$(GJ)_e \frac{\partial^3 w}{\partial x^2 \partial y} + \text{Inertia terms} = M_r - M_l \quad (5)$$

where

$$(GJ)_e = GJ + E C_w \left(\frac{n\pi y}{W} \right)^2 \quad (6)$$

is the required effective torsional stiffness factor. Since it is expected that the effect of the stringers on the panel dynamics will be most pronounced for deflections with one half wave in the y direction, n is assumed equal to unity in

equation (6). This means that the effective stringer torsional stiffness will be correct for panel deflections with one half wave in the y direction, but will be underestimated for deflections with more than one half wave in the y direction.

2.3 Vibration Modes and Random Response

The stiffness and mass matrices for an approximate representation of the multi-bay panel may now be established from the results of Sections 2.1 and 2.2. Once these are available, the vibration modes for the panel are calculated by setting up the eigenvalue problem

$$(K - \lambda M) \vec{x} = 0 \quad (7)$$

where K and M are the system stiffness and mass matrices and $\lambda = \mu \omega^2 a^4 / 1680 D$ is the non-dimensional eigenvalue, and carrying out the computation on the digital computer. This will be done for a particular example in Section 3.0.

These stiffness and mass matrices may also be employed in determining the panel response to a random excitation field. The only additional requirement is a suitable matrix representation for the structural damping in the panel. In the following work, the panel damping matrix P is approximated by

$$P = i g K \quad (8)$$

where g is a small constant. It may be noted that equation (8) is a commonly adopted approximation for structural damping that, in effect, assumes that the damping forces are proportional to, and 90 degrees out of phase with, the elastic restoring forces in a structure. This type of approximation is justified in that the actual mechanism of damping in structures is largely unknown, and only the overall energy dissipation can be accurately represented.

Using equation (8), the matrix equation governing the panel response

then becomes

$$k M \frac{d^2 \vec{x}}{dt^2} + (1 + ig) K \vec{x} = \vec{f}(t) \quad (9)$$

Where $k = \mu a^4/1680 D$ and \vec{x} and \vec{f} are the nondimensional displacement and load vectors for the system, respectively. In this case, \vec{f} will be a discrete set of random loads that approximates the spatially distributed loading acting on the panel.

Following the method developed in Reference 5, equation (9) is first Fourier transformed to give

$$\left[(1 + ig) K - \alpha M \right] \vec{X} = \vec{F} \quad (10)$$

where $\alpha = \mu \omega^2 a^4/1680 D$ and $\vec{X}(\omega)$ and $\vec{F}(\omega)$ are the "truncated" Fourier transforms of $\vec{x}(t)$, respectively. Then inverting equation (10) yields

$$\vec{X} = B \vec{F} = (B_R + i B_I) \vec{F} \quad (11)$$

where

$$B_R = \left[I - \alpha K^{-1} M \right] \left[(1+g^2) K - 2 \alpha M + \alpha^2 M K^{-1} M \right]^{-1} \quad (12)$$

$$B_I = -g \left[(1 + g^2) K - 2 \alpha M + \alpha^2 M K^{-1} M \right]^{-1}$$

Writing equation (11) in index notation and combining with its complex conjugate yields

$$X_i X_i^* = \sum_j \sum_k B_{ij} B_{ik}^* F_j F_k^* \quad (13)$$

Dividing by $2T$, where T is the characteristic time used in the "truncated"

Fourier transforms, and taking the limit as $T \rightarrow \infty$, yields the power spectral density for the i^{th} generalized co-ordinate as

$$S_{x_{ii}}(\omega) = \lim_{T \rightarrow \infty} \frac{x_i x_i^*}{2T} = \sum_j \sum_k B_{ij} B_{ik}^* S_{F_{jk}}(\omega) \quad (14)$$

where

$$S_{F_{jk}}(\omega) = \lim_{T \rightarrow \infty} \frac{F_j F_k^*}{2T}$$

is the cross-spectral density for the discretized random loads $\vec{f}(t)$. It may be shown (Ref. 5) that $S_{F_{jk}} = S_{F_{kj}}^*$, so that equation (14) may be simplified to

$$S_{X_{ii}}(\omega) = \sum_{j=1}^N \left| B_{ij} \right|^2 R^{\prime\ell} \left[S_{F_{jj}}(\omega) \right] + 2 \sum_{j=1}^{k-1} \sum_{k=2}^N \left\{ \left[B_{Rij} B_{Rik} + B_{Iij} B_{Iik} \right] \times \right. \\ \left. R^{\prime\ell} \left[S_{F_{jk}}(\omega) \right] + \left[B_{Rij} B_{Iik} - B_{Rik} B_{Iij} \right] I^{\prime m} \left[S_{F_{jk}}(\omega) \right] \right\} \quad (15)$$

where $R^{\prime\ell}$ and $I^{\prime m}$ denote real and imaginary parts, respectively. The mean square amplitude for the i^{th} displacement is then the integral of this power spectral density over all frequencies

$$X_i^2 = 2 \int_0^{\infty} S_{x_{ii}}(\omega) d\omega \quad (16)$$

The procedure then is to calculate the power spectral densities for particular values of frequency from equation (15) and evaluate equation (16) by some numerical integration procedure such as Simpson's rule.

3.0 EXAMPLE APPLICATION

The analysis for the five-bay, stringer-stiffened panel illustrated in Figure 2 is presented in the following. The edges $y = 0$ and $y = W$ represent

the ribs and are considered to be clamped. The overall length L is divided into five equal bays by the stringers, as shown. The edges $x = 0$ and $x = L$ are also assumed to be clamped. Since the stringers in most aerospace structures are usually much stiffer in bending than in torsion, it is assumed explicitly that the stringers are infinitely stiff in bending but have finite torsional stiffness and rotational inertia. The numerical calculations are carried out for a typical panel having the following properties

$$\begin{aligned} E &= 10^7 \text{ psi}, & \nu &= 0.3, & L &= 45.0 \text{ in} \\ W &= 16.5 \text{ in}, & d &= 1.0 \text{ in}, & e &= 0.75 \text{ in} \\ \rho &= 0.000259 \text{ lb sec}^2/\text{in}^4, & h &= 0.052 \text{ in} \end{aligned} \tag{17}$$

The quantities required in equation (6) then become $J = 0.00010 \text{ in}^4$, $C_w = 0.0055 \text{ in}^6$, and $I = 0.031 \text{ in}^4$.

The two finite element representations used to approximate the five-bay panel are illustrated in Figure 5. The procedure for building up the system matrices (stiffness and mass) for these representations is quite standard and need only be described briefly.

The three generalized co-ordinates ψ_x , ψ_y , and w at the plate element corners are made continuous at all element corner junctions, and the sum of corresponding corner moments and shears M_x , M_y , and V (ordinary plus D'Alembert ones) are set equal to the applied loads for the response problem or to zero for the eigenvalue problem. There are no degrees of freedom on the outer edges of the panel because of the clamped boundary conditions, and there is only one degree of freedom ψ_x at each corner junction on a stringer because of the assumption of no stringer bending. At all other corner junctions, there are 3 degrees of freedom ψ_x , ψ_y , and w . Hence, the 3×3 grid per bay representation shown in Figure 5a has 68 degrees of freedom, and the 4×4 case shown in Figure 5b has 147.

Stringer torsional elements are added to the grid works shown in Figure 5 along the lines marked "stringers". These elements are the same length as the plate elements, i.e. $W/3$ or $W/4$ for Figure 4a or 4b, respectively, so that the stringer element rotations θ may be set equal to the plate element slopes ψ_x . The stringer rotations are taken to be zero at $y = 0$ and W . The stringer stiffnesses and masses calculated from equations (3) and (6) are added to the appropriate places in the system stiffness and mass matrices generated from the plate element matrices.

3.1 Vibration Modes

Calculations of eigenvalues and eigenvectors for the dynamic systems generated by the foregoing process were carried out on the National Research Council Computing Center IBM 360-50 Digital Computer. It should be noted that, whereas the 68 degree of freedom model could be handled directly, the 147 degree of freedom model had to be broken down into four smaller systems by using symmetry. That is, since the panel shown in Figure 5 exhibits symmetry in both the x and y directions, all its vibration modes are either symmetric or antisymmetric in these directions. Hence, all modes may be classified into four categories, which are the four combinations of symmetry in the two directions. The numbers of degrees of freedom obtained in each sub-problem are as follows:

	<u>Mode Shape</u>	<u>Degrees of Freedom</u>
(i)	Symmetric in both x and y	42
(ii)	Symmetric in x , antisymmetric in y	33
(iii)	Antisymmetric in x , symmetric in y	41
(iv)	Antisymmetric in both x and y	31

The numerical results are shown in Tables III and IV. Table III gives a comparison of the results obtained from the 3×3 grid/bay representation and the 4×4 grid/bay representation, with the effect of stringers included in both. The corresponding mode shapes (eigenvectors), as obtained

from the 4×4 grid/bay representation, are plotted in Figures 6 to 23. The heavy lines in these Figures represent the outer clamped boundaries of the panel and the four stringers across it. The light curves show the panel deflection at the junctions of the plate elements, and the dashed curves represent the nodal lines. The panel deflection curves were obtained by fitting third-order polynomials to the appropriate eigenvector components (ψ_x or ψ_y and w) of adjacent control points.

The vibration modes occur in distinct groups of five each because there are five bays in the panel. These groups are labelled arbitrarily A, B, C, etc., for identification purposes, as shown in Column 1 of Table III. The symmetry character of each mode is indicated in Columns 4 and 5, where the symbols S and A stand for symmetric and antisymmetric, respectively. The predominant number of half waves present in the mode shapes in each direction are also indicated by the numbers in these columns.

As shown in the Figures, the fifth mode in each group has a mode shape with zero slope across each stringer. Hence, in these modes each bay vibrates effectively as though the stringers were clamped edges, and the frequencies may be compared with those predicted for a clamped plate the size of each bay. Such a prediction is shown in Column 6 of Table III as obtained from Warburton's Rayleigh solutions (Ref. 6).

The comparison of the fifth frequency in each group, with the Warburton results, is very interesting. For the mode groups A, D, E, and G, these frequencies appear to converge towards the Warburton result as the finite element modelling is increased from the 3×3 to the 4×4 grid/bay representation. On the other hand, for groups B, C, and F, they appear to diverge slightly from the Warburton results. Presumably, a finer grid work of elements would be required to make these latter groups converge to the correct result. However, it may be noted that the maximum error in these frequencies, as predicted by the 4×4 grid/bay representation, is only 15 percent. It is expected that the accuracy of the other four frequencies in each group would be

the same or better than that of the fifth. Hence, it appears that the first 35 vibration frequencies for the five-bay panel are predicted to within 15 percent by the 4×4 grid/bay finite element representation.

Only the fifth frequency in each of the higher groups H to N are presented in Table III. It is clear that these predictions are far less accurate than the lower ones, although they are the correct order of magnitude.

The modes shapes associated with the frequencies in Table III, and exhibited in Figures 6 to 23, also reveal some interesting effects. The first ten modes are very clear, having one or two half waves in the y direction. However, the next four modes exhibit unusual nodal patterns in the x direction. These are fundamentally different from the straight nodal lines that would occur if the panel edges $y = 0$ and W were simply supported. In the present problem, the clamped boundary conditions preclude the possibility of a separable solution for the panel deflection that can always be obtained for the simply supported case. Hence, the unusual nodal patterns found herein may be associated with these clamped boundary conditions. As shown in the Figures, more non-straight nodal lines in the x direction are revealed in some of the higher modes. In particular, see Figures 21 to 23.

Numerical results were also obtained for the five-bay panel frequencies with the effect of stringers neglected, i.e. for the panel simply supported at the stringers. These were obtained from the 4×4 grid/bay representation and are shown in Table IV along with the results for stringers. It is seen that including the effect of the stringers pushes up the lower frequencies in each group. The fifth frequency is not changed because the stringers are effectively clamped for the modes associated with these frequencies, as noted earlier. Hence, the effect of the stringers is to decrease the frequency bandwidth of each modal group.

3.2 Random Response

The calculation of the panel response to a random pressure loading is

also carried out using the finite element representations. Numerical results are presented for the particular excitation known as plane wave propagation of acoustic white noise. This type of random loading is of special interest because it may be considered as an idealization of the pressure fields induced downstream by jet engine exhausts. Hence, many parts of a modern jet aircraft such as the rear fuselage, horizontal stabilizer, and vertical rudder, encounter this type of noise excitation.

Plane wave propagation of white acoustic noise is characterized by the following cross-spectral density (Ref. 5)

$$S(\xi, \omega) = \left. \begin{aligned} & \frac{\overline{p_0^2}}{\omega_c} \exp \left[-\frac{i\omega\xi}{c} \right] && \text{for } |\omega| \leq \omega_c \\ & = 0 && \text{for } |\omega| > \omega_c \end{aligned} \right\} \quad (18)$$

where

$\overline{p_0^2}$ = mean square amplitude of pressure, (psi)

ω_c = the cut-off frequency, which is assumed large, (rad/sec)

c = acoustic propagation speed

ξ = distance between field points (measured in the direction of propagation).

The direction of noise propagation is taken to be down the panel in the x direction (Fig. 5).

The numerical calculations are carried out for the 3×3 grid/bay representation shown in Figure 5a. The distributed acoustic loading on the panel is approximated by a set of concentrated transverse shear loads acting at the finite element corner junctions, points 1 to 27 in the Figure. The root mean square amplitude of each concentrated load will be $ab \sqrt{\overline{p_0^2}}$, i.e., equal

to the rms acoustic pressure times the area of one element. It is assumed that the cross-spectral density functions for these concentrated loads are given by equation (18) with ξ measured between the loads; that is

$$S_{Fjk}(\omega) = \frac{a^2 b^2 \overline{p_0^2}}{\omega_c} \exp \left[-\frac{i\omega}{c} (\xi_k - \xi_j) \right] \quad (19)$$

where ξ_j is the x co-ordinate of point j. The foregoing approximations will be reasonably good as long as the acoustic wave lengths associated with the frequencies that dominate the panel response are long compared with the finite element width a. This will indeed be the case for the present problem, since the predominant panel frequencies are from 100 to 500 cps.

Since the plane wave noise propagation does not vary in the y direction, the panel response must be symmetric in y. Hence, by using this symmetry condition, the 68 degree of freedom system associated with Figure 5a may be reduced to 34 degrees of freedom. The numerical calculations involved in equations (15) and (16) are carried out for this 34 degree of freedom system, and the results are presented in Figures 24 to 37 for a structural damping of $g = 0.02$. Note that the calculations were not continued above 500 cps, since the major part of the panel response occurs at frequencies below this value.

Figures 24 to 33 show the power spectral densities for the displacements at points 1, 3, 7, 9, 13, 15, 19, 21, 25, and 27 on the panel (Fig. 5a). Since the panel response is symmetric in y, the power spectral densities for displacements at the symmetric points 2 to 28 will be identical with Figures 24 to 33, respectively. The three relatively wide peaks exhibited in these Figures are clearly recognizable as being associated with modal groups A, C, D, and G shown in Table III. Furthermore, some of the small individual peaks in the Figures are recognizable as being associated with individual modes. For example, in Figure 26 the five small peaks from 103 to 141 cps are associated with the five individual modes in group A, and in Figure 25 the five peaks from 274 to 335 cps are associated with the five modes in group D. On the other

hand, the response of modal group G appears to be dominated by the three peaks at 416, 427 and 443 cps.

Modal group C, which should also be excited by the acoustic noise, is not recognizable in these Figures because the panel modes of this group have modal lines very close to the control points 1 to 28 (see Fig. 16 to 18). Hence, the response associated with these modes at these points is too small to show up in the displacement power spectral density curves. The modal groups B, E, and F are not recognizable in the Figures, since they are antisymmetric in y and are not excited by the noise field.

Figure 34 shows the power spectral density for the panel slope in the x direction, ψ_x , at the control point 27 (Fig. 5a). It may be noted that this power spectral density curve is very similar to that for the displacement at point 27 (Fig. 33). In particular, the shape of the first response band from 103 to 141 cps is almost identical in the two Figures. It is interesting to note that, whereas some of the individual peaks in the second response band from 274 to 335 cps were not evident in Figure 33, they show up clearly in Figure 34. The corresponding results for the other control points were very similar and hence are not presented herein.

Figure 35 shows the power spectral density for the panel slope in the y direction, ψ_y , at the same control point 27, for comparison. The first response band from 103 to 141 cps is very similar to that in Figure 33. However, the second response band from 274 to 335 cps is somewhat different in that relative to the first band it is about one order of magnitude larger than it was in Figure 33, and exhibits individual peaks at 274, 317 and 335 cps that were absent in Figure 33.

Actually, panel modes that have several half waves in the y direction should have larger power spectral densities for slope ψ_y than for displacement w compared with those with fewer waves in the y direction. Hence, the modal responses associated with group C should be emphasized more in Figure 35 than those associated with group D (Table III). However, it appears that the

response due to both groups has been increased in Figure 35. This result must be associated with the fact that the 3×3 grid/bay finite element representation for the panel does not adequately separate the modes of groups C and D. In other words, the mode shapes predicted by the 3×3 grid/bay representation for modes 11 to 20 (273.84 to 335.23 cps) all had about equal "waviness" in the y direction, whereas (as shown in Fig. 11 to 15) the 4×4 grid/bay representation did clearly separate the modes into groups C and D. Hence, the fact that some of the modes of group D are emphasized in Figure 35 must be attributed to this limitation in the 3×3 grid/bay representation. Finally, it may be noted that the response of modal group G (410 to 453 cps) is increased in Figure 35 as expected, since the modes in group G have three half waves in the y direction.

The mean square response for each degree of freedom was also obtained by numerical integration of its power spectral density curve, using Simpson's rule. This was done simultaneously with the calculation of the power spectra. A frequency step size of 1.0 cps was used within the response bands, and one of 10.0 cps was used between the bands.

The results in terms of root mean square amplitude are shown in Figures 36 and 37. Figure 36 shows the longitudinal distribution of the rms panel response. It is interesting to note that this response is not symmetric with respect to the centre bay and, in particular, the maximum amplitude occurs in the last downstream bay. These results are a consequence of the directionality of the excitation field. Figure 37 shows the lateral distributions of the rms panel response in the centre and last bays. These curves indicate that the panel response is dominated by modes with one half wave parallel to the stringer. The relative flatness of the top of these curves is evidence of the presence of higher modes, even though their contribution is small.

4.0 CONCLUDING REMARKS

A finite element approach to the analysis of continuous skin-stringer

panels has been presented. The method was illustrated in the calculation of vibration modes and random response of a five-bay stringer-stiffened panel with all outer edges clamped. The panel skin was represented by finite plate elements and the stringers, which were assumed infinitely stiff in bending, were represented by beam torsional elements.

The panel vibration modes were obtained from both a 3×3 and a 4×4 grid of plate elements per bay. It was estimated that the first 35 panel frequencies obtained from the latter representation were within 15 percent of the correct values. The vibration modes occurred in distinct groups with five similar modes in each, the number five corresponding to the number of panel bays. A comparison of the results obtained with and without the effect of stringers included, showed that the stringers effectively reduce the frequency bandwidth of each group of five modes.

The response of the panel to plane wave propagation of acoustic noise (propagating normal to the stringers) was also obtained, using the 3×3 grid/bay of finite elements. The resulting response power spectral densities were found to be fundamentally different from those associated with single span panels. These power spectra did not have widely separated peaks, but rather the peaks tended to be squeezed into groups corresponding to the groupings of natural frequencies for the panel. The individual modal responses within each group were blurred together, indicating that the response cannot be thought of as the summation of independent modal responses.

5.0 REFERENCES

1. Lin, Y.K. Probabilistic Theory of Structural Dynamics. McGraw Hill Book Company, New York, N.Y., 1967.
2. Mercer, C.A.
Seavey, C. Prediction of Natural Frequencies and Normal Modes of Skin-Stringer Panel Rows. J. Sound Vibration, Vol. 6, No. 1, 1967, pp. 149-162.

3. Lindberg, G.M. Lumped Parameter Methods Applied to Elastic Vibrations.
Ph. D. Thesis, University of Cambridge, Cambridge, England, Nov. 1963.
4. Zienkiewicz, O.C. The Finite Element Method in Structural and Continuum Mechanics.
McGraw Hill Book Company, London, England, 1967.
5. Olson, Mervyn D. A Numerical Approach to Random Response Problems.
NRC NAE Aero. Report LR-479, National Research Council of Canada, Ottawa, Ont., Apr. 1967.
6. Warburton, G.B. The Vibration of Rectangular Plates.
Proc. Institute of Mechanical Engineers, London, England, Vol. 168, 1954, pp. 371-381.

M_{x1}	$\frac{2}{3m} + \frac{2(1-\nu)m}{15}$																	ψ_{x1}
M_{y1}	$\frac{\nu}{2}$	$\frac{2m}{3} + \frac{2(1-\nu)}{15m}$																ψ_{y1}
$V_1 a$	$\frac{1}{m} + \frac{(1+4\nu)m}{10}$	$m^2 + \frac{(1+4\nu)}{10}$	$\frac{2m^3 + \frac{2}{m}}{(7-2\nu)m} + \frac{2}{5}$															$\frac{w_1}{a}$
M_{x2}	$\frac{1}{3m} - \frac{(1-\nu)m}{30}$	0	$\frac{1}{m} + \frac{(1-\nu)m}{10}$	$\frac{2}{3m} + \frac{2(1-\nu)m}{15}$														ψ_{x2}
M_{y2}	0	$\frac{m}{3} - \frac{2(1-\nu)}{15m}$	$\frac{m^2 - (1+4\nu)}{2} - \frac{(1+4\nu)}{10}$	$-\frac{\nu}{2}$	$\frac{2m}{3} + \frac{2(1-\nu)}{15m}$													ψ_{y2}
$V_2 a$	$\frac{-1}{m} - \frac{m(1-\nu)}{10}$	$\frac{m^2 - (1+4\nu)}{2} - \frac{(1+4\nu)}{10}$	$\frac{m^3 - \frac{2}{m}}{(7-2\nu)m} - \frac{(1 + \frac{(1+4\nu)m}{10})}{m^2 + \frac{(1+4\nu)}{10}}$	$\frac{2m^3 + \frac{2}{m}}{(7-2\nu)m} + \frac{2}{5}$														$\frac{w_2}{a}$
M_{x3}	$\frac{1}{6m} + \frac{(1-\nu)m}{30}$	0	$\frac{1}{2m} - \frac{(1-\nu)m}{10}$	$\frac{1}{3m} - \frac{2(1-\nu)m}{15}$	0	$\frac{-1}{2m} + \frac{(1+4\nu)m}{10}$	$\frac{2}{3m} + \frac{2(1-\nu)m}{15}$											ψ_{x3}
M_{y3}	0	$\frac{m}{6} + \frac{(1-\nu)}{30m}$	$\frac{m^2 - (1-\nu)}{2} - \frac{(1-\nu)}{10}$	0	$\frac{m}{3} - \frac{(1-\nu)}{30m}$	$m^2 + \frac{(1-\nu)}{10}$	$\frac{\nu}{2}$	$\frac{2m}{3} + \frac{2(1-\nu)}{15m}$										ψ_{y3}
$V_3 a$	$\frac{-1}{2m} + \frac{(1-\nu)m}{10}$	$-\frac{m^2 + (1-\nu)}{2} + \frac{(1-\nu)}{10}$	$\frac{-m^3 - \frac{1}{m}}{(7-2\nu)m} + \frac{(1+4\nu)m}{5}$	$-\frac{1}{2m} + \frac{(1+4\nu)m}{10}$	$-\left(m^2 + \frac{(1-\nu)}{10}\right)$	$\frac{-2m^3 + \frac{1}{m}}{(7-2\nu)m} - \frac{(1 + \frac{(1+4\nu)m}{10})}{m^2 + \frac{(1+4\nu)}{10}}$	$\frac{2m^3 + \frac{2}{m}}{(7-2\nu)m} + \frac{2}{5}$											$\frac{w_3}{a}$
M_{x4}	$\frac{1}{3m} - \frac{2(1-\nu)m}{15}$	0	$\frac{1}{2m} - \frac{(1+4\nu)m}{10}$	$\frac{1}{6m} + \frac{(1-\nu)m}{30}$	0	$\frac{-1}{2m} + \frac{(1-\nu)m}{10}$	$\frac{1}{3m} - \frac{(1-\nu)m}{30}$	0	$-\left(\frac{1}{m} + \frac{(1-\nu)m}{10}\right)$	$\frac{2}{3m} + \frac{2(1-\nu)m}{15}$								ψ_{x4}
M_{y4}	0	$\frac{m}{3} - \frac{(1-\nu)}{30m}$	$m^2 + \frac{(1-\nu)}{10}$	0	$\frac{m}{6} + \frac{(1-\nu)}{30m}$	$\frac{m^2 - (1-\nu)}{2} - \frac{(1-\nu)}{10}$	0	$\frac{m}{3} - \frac{2(1-\nu)}{15m}$	$-\frac{m^2 + (1+4\nu)}{2} + \frac{(1+4\nu)}{10}$	$-\frac{\nu}{2}$	$\frac{2m}{3} + \frac{2(1-\nu)}{15m}$							ψ_{y4}
$V_4 a$	$\frac{1}{2m} - \frac{(1+4\nu)m}{10}$	$-\left(m^2 + \frac{(1-\nu)}{10}\right)$	$\frac{-2m^3 + \frac{1}{m}}{(7-2\nu)m} - \frac{(1+4\nu)m}{5}$	$\frac{1}{2m} - \frac{(1-\nu)m}{10}$	$-\frac{m^2 + (1-\nu)}{2} + \frac{(1-\nu)}{10}$	$\frac{-m^3 - \frac{1}{m}}{(7-2\nu)m} + \frac{(1+4\nu)m}{5}$	$\frac{1}{m} + \frac{(1-\nu)m}{10}$	$-\frac{m^2 + (1+4\nu)}{2} + \frac{(1+4\nu)}{10}$	$\frac{m^3 - \frac{2}{m}}{(7-2\nu)m} - \frac{(1+4\nu)m}{5}$	$\frac{1}{m} + \frac{(1+4\nu)m}{10}$	$-\left(m^2 + \frac{(1+4\nu)}{10}\right)$	$\frac{2m^3 + \frac{2}{m}}{(7-2\nu)m} + \frac{2}{5}$						$\frac{w_4}{a}$

$m = a/b$
 $\nu = \text{POISSON'S RATIO}$

SYMMETRICAL

= 2 D

TABLE I

STIFFNESS MATRIX FOR FINITE PLATE ELEMENT

M_{x1}^*	$\frac{80}{m}$												ψ_{x1}
M_{y1}^*	$\frac{63}{m^2}$	$\frac{80}{m^3}$											ψ_{y1}
$V_1^* a$	$\frac{461}{m}$	$\frac{461}{m^2}$	$\frac{3454}{m}$										$\frac{w_1}{a}$
M_{x2}^*	$-\frac{60}{m}$	$-\frac{42}{m^2}$	$-\frac{274}{m}$	$\frac{80}{m}$									ψ_{x2}
M_{y2}^*	$\frac{42}{m^2}$	$\frac{40}{m^3}$	$\frac{199}{m^2}$	$-\frac{63}{m^2}$	$\frac{80}{m^3}$								ψ_{y2}
$V_2^* a$	$\frac{274}{m}$	$\frac{199}{m^2}$	$\frac{1226}{m}$	$-\frac{461}{m}$	$\frac{461}{m^2}$	$\frac{3454}{m}$							$\frac{w_2}{a}$
M_{x3}^*	$-\frac{30}{m}$	$-\frac{28}{m^2}$	$-\frac{116}{m}$	$\frac{40}{m}$	$-\frac{42}{m^2}$	$-\frac{199}{m}$	$\frac{80}{m}$						ψ_{x3}
M_{y3}^*	$-\frac{28}{m^2}$	$-\frac{30}{m^3}$	$-\frac{116}{m^2}$	$\frac{42}{m^2}$	$-\frac{60}{m^3}$	$-\frac{274}{m^2}$	$\frac{63}{m^2}$	$\frac{80}{m^3}$					ψ_{y3}
$V_3^* a$	$\frac{116}{m}$	$\frac{116}{m^2}$	$\frac{394}{m}$	$-\frac{199}{m}$	$\frac{274}{m^2}$	$\frac{1226}{m}$	$-\frac{461}{m}$	$-\frac{461}{m^2}$	$\frac{3454}{m}$				$\frac{w_3}{a}$
M_{x4}^*	$\frac{40}{m}$	$\frac{42}{m^2}$	$\frac{199}{m}$	$-\frac{30}{m}$	$\frac{28}{m^2}$	$\frac{116}{m}$	$-\frac{60}{m}$	$-\frac{42}{m^2}$	$\frac{274}{m}$	$\frac{80}{m}$			ψ_{x4}
M_{y4}^*	$-\frac{42}{m^2}$	$-\frac{60}{m^3}$	$-\frac{274}{m^2}$	$\frac{28}{m^2}$	$-\frac{30}{m^3}$	$-\frac{116}{m^2}$	$\frac{42}{m^2}$	$\frac{40}{m^3}$	$-\frac{199}{m^2}$	$-\frac{63}{m^2}$	$\frac{80}{m^3}$		ψ_{y4}
$V_4^* a$	$\frac{199}{m}$	$\frac{274}{m^2}$	$\frac{1226}{m}$	$-\frac{116}{m}$	$\frac{116}{m^2}$	$\frac{394}{m}$	$-\frac{274}{m}$	$-\frac{199}{m^2}$	$\frac{1226}{m}$	$\frac{461}{m}$	$-\frac{461}{m^2}$	$\frac{3454}{m}$	$\frac{w_4}{a}$

SYMMETRICAL

$m = a/b$

$= \frac{\mu \omega^2 a^4}{25200}$

TABLE II

MASS MATRIX FOR FINITE PLATE ELEMENT

TABLE III

FIVE-BAY PANEL VIBRATION FREQUENCIES

(Effect of Stringers Included)

Mode Group	3 × 3 grid/bay 68 deg of freedom (cps)	4 × 4 grid/bay 147 deg of freedom (cps)	symmetry and half waves in y dir'n	symmetry and half waves/bay in x dir'n	Warburton result (cps)
A	103.42	105.06	S - 1	S - 1	152.4
	112.35	114.36	S - 1	A - 1	
	124.60	127.17	S - 1	S - 1	
	136.14	139.38	S - 1	A - 1	
	141.18	144.77	S - 1	S - 1	
B	177.37	174.82	A - 2	S - 1	207.2
	180.70	178.21	A - 2	A - 1	
	185.11	182.71	A - 2	S - 1	
	188.97	186.66	A - 2	A - 1	
	190.53	188.25	A - 2	S - 1	
C	288.42	281.41	S - 3	S - 1	303.4
	294.78	282.47	S - 3	A - 1	
	295.88	284.18	S - 3	S - 1	
	299.67	287.01	S - 3	A - 1	
	299.17	287.03	S - 3	S - 1	
D	273.84	280.37	S - 1	A - 2	391.1
	303.23	304.16	S - 1	S - 2	
	317.01	332.59	S - 1	A - 2	
	330.42	358.89	S - 1	S - 2	
	335.23	370.60	S - 1	A - 2	
E	558.78	454.61	A - 4	S - 1	439.8
	558.90	454.83	A - 4	A - 1	
	559.02	455.02	A - 4	S - 1	
	559.09	455.13	A - 4	A - 1	
	559.12	455.17	A - 4	S - 1	
F	354.97	346.39	A - 2	A - 2	444.2
	364.68	356.11	A - 2	S - 2	
	376.94	368.47	A - 2	A - 2	
	387.22	378.97	A - 2	S - 2	
	391.26	383.16	A - 2	A - 2	
G	410.50	454.08	S - 3	A - 2	534.0
	415.96	459.54	S - 3	S - 2	
	426.96	466.84	S - 3	A - 2	
	443.00	473.88	S - 3	S - 2	
	452.64	477.45	S - 3	A - 2	
H	-	738.51	S - 5	S - 1	614.2
I	-	578.94	A - 4	A - 2	663.1
J	-	662.65	S - 1	S - 3	749.8
K	-	629.30	A - 2	S - 3	803.3
L	-	861.35	S - 5	A - 2	831.4
M	-	800.87	S - 3	S - 3	891.1
N	-	831.58	A - 4	S - 3	1016.0

TABLE IV
EFFECT OF STRINGERS ON PANEL FREQUENCIES
(Obtained from 4×4 grid/bay representation)

Mode Group	Panel Frequencies without effect of stringers (cps)	Panel Frequencies including effect of stringers (cps)
A	89.154	105.06
	101.78	114.36
	119.20	127.17
	136.54	139.38
	144.77	144.77
B	155.11	174.82
	162.44	178.21
	172.98	182.71
	183.47	186.66
	188.25	188.25
C	263.79	281.41
	268.96	282.47
	276.18	284.18
	283.92	287.01
	287.03	287.03
D	262.78	280.37
	291.36	304.16
	325.22	332.59
	356.43	358.89
	370.60	370.60
E	453.81	454.61
	454.50	454.83
	454.92	455.02
	455.11	455.13
	455.17	455.17
F	304.81	346.39
	325.36	356.11
	350.79	368.47
	373.42	378.97
	383.16	383.16
G	405.02	454.08
	422.80	459.54
	445.91	466.84
	467.56	473.88
	477.45	477.45

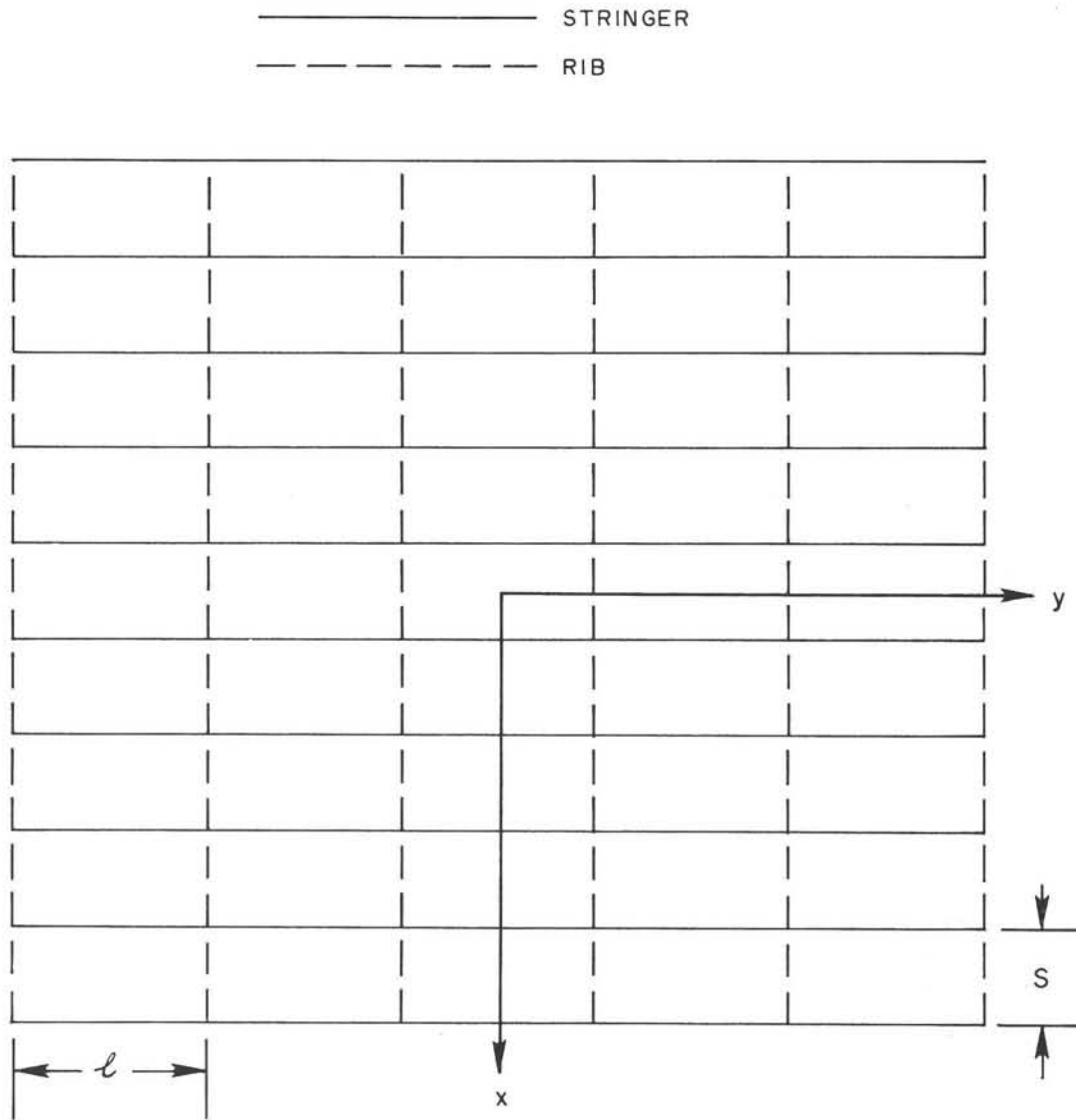


FIG. 1 IDENTICALLY CONSTRUCTED PANELS

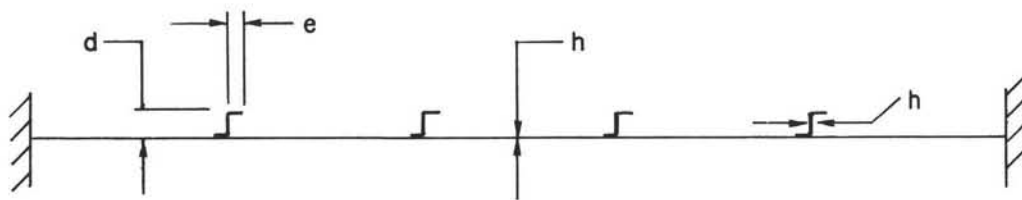
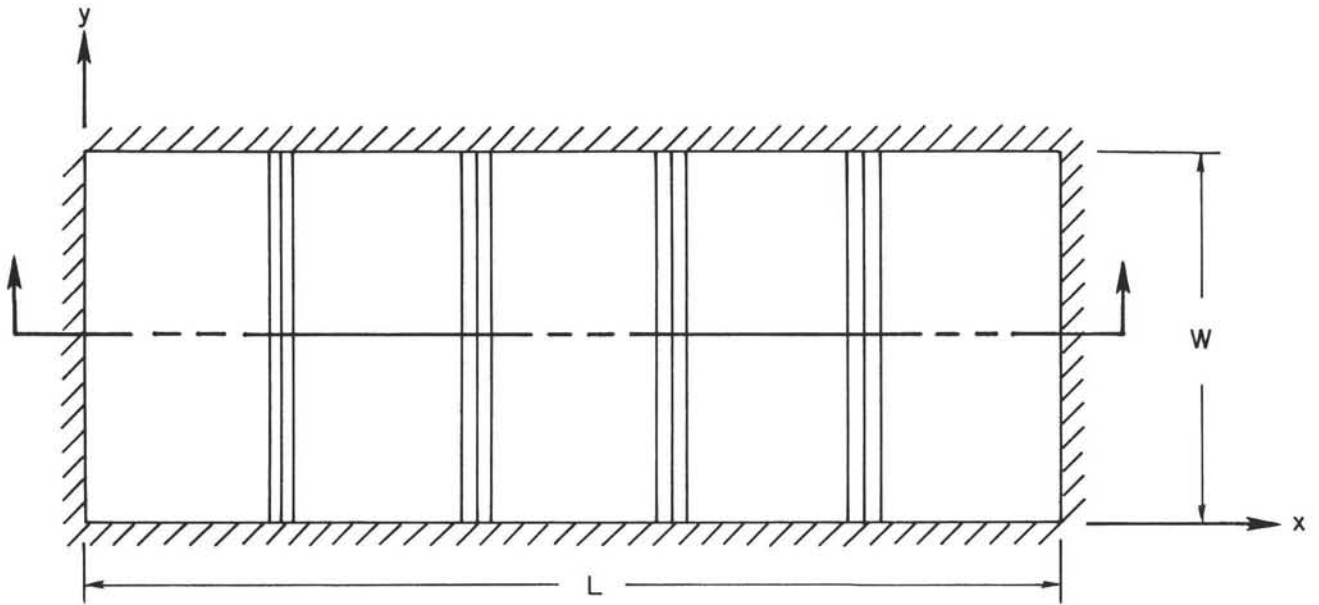


FIG. 2 FIVE-BAY STRINGER-STIFFENED PANEL

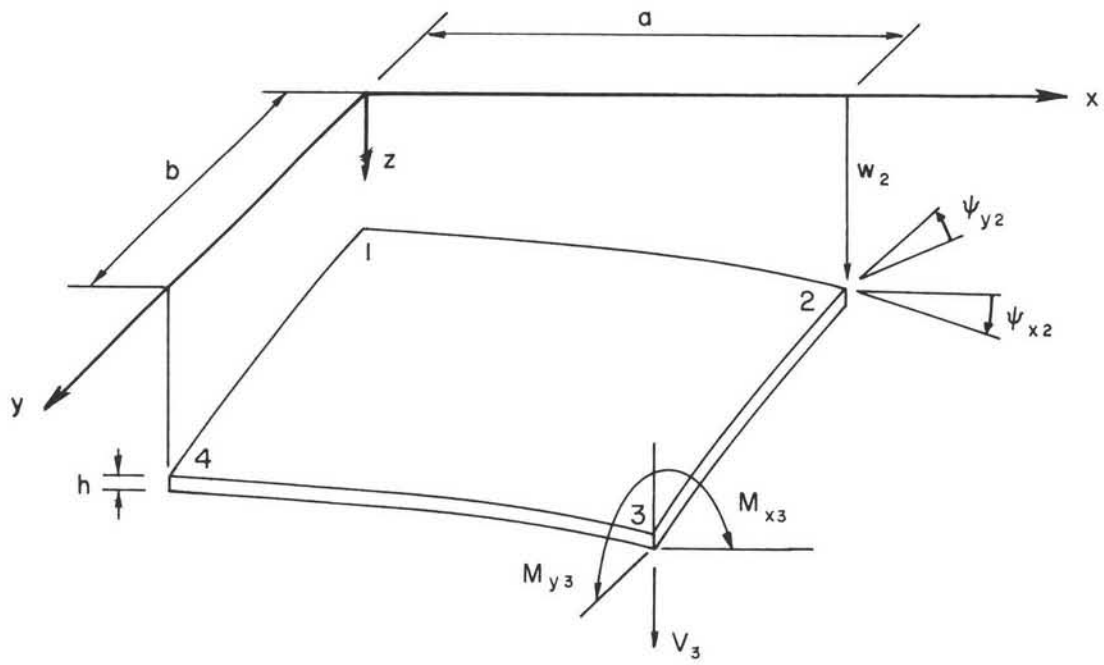


FIG. 3

PLATE ELEMENT

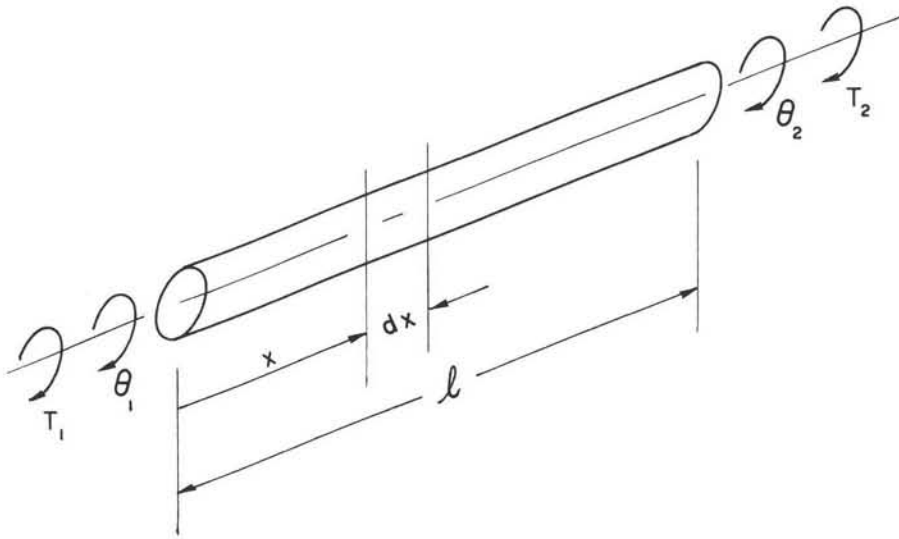
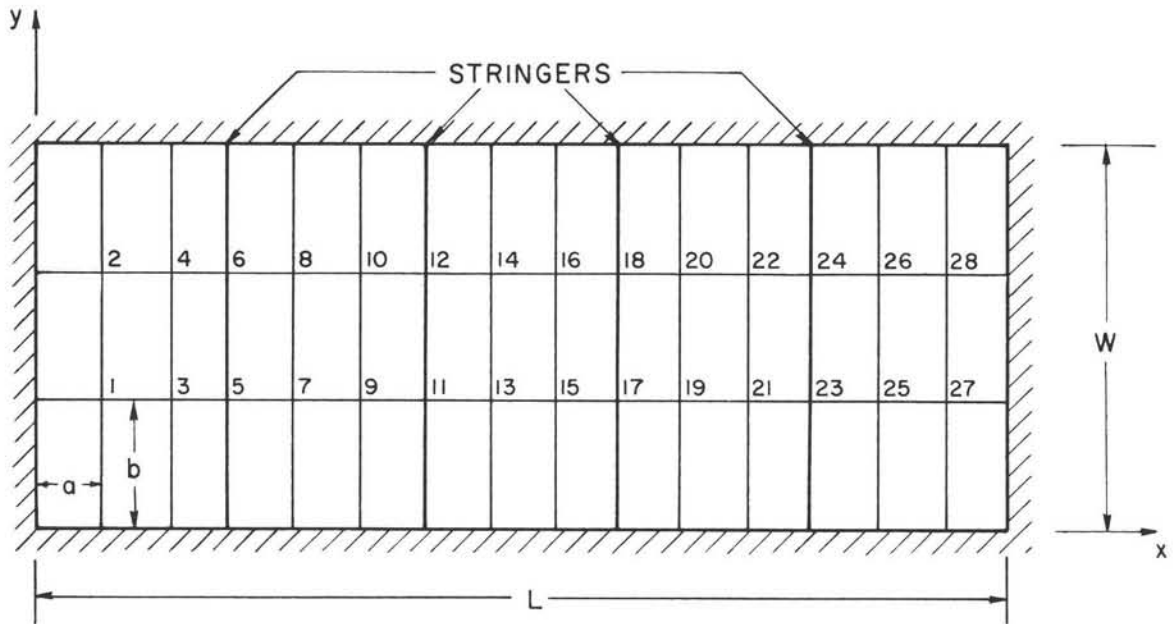
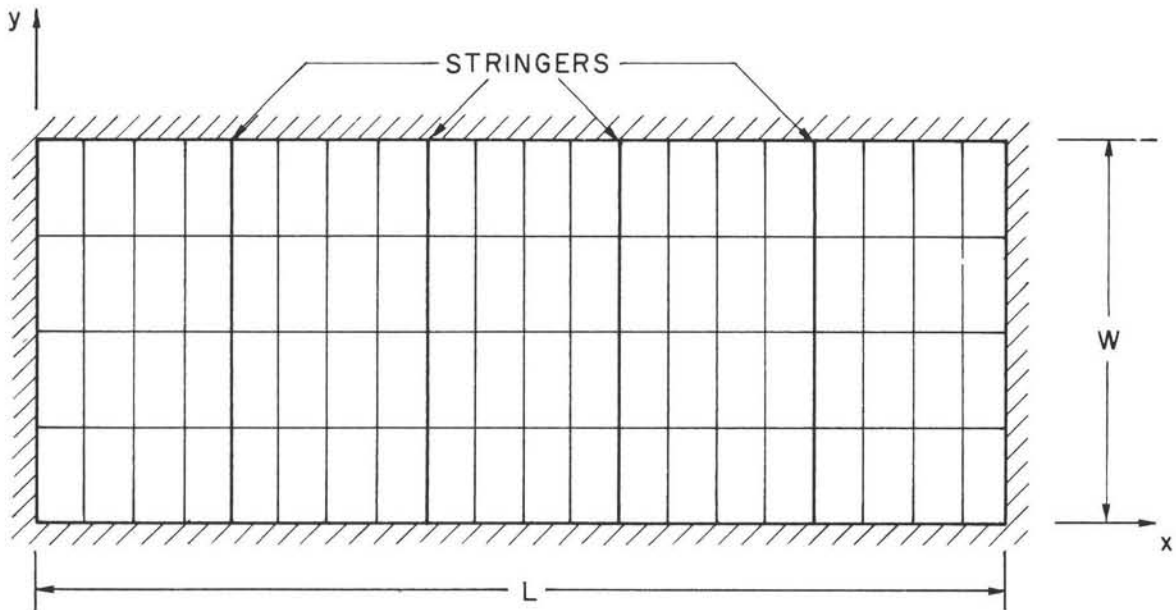


FIG. 4

TORSIONAL BEAM ELEMENT



3 x 3 GRID PER BAY REPRESENTATION



4 x 4 GRID PER BAY REPRESENTATION

FIG. 5
FINITE ELEMENT REPRESENTATIONS FOR FIVE-BAY PANEL

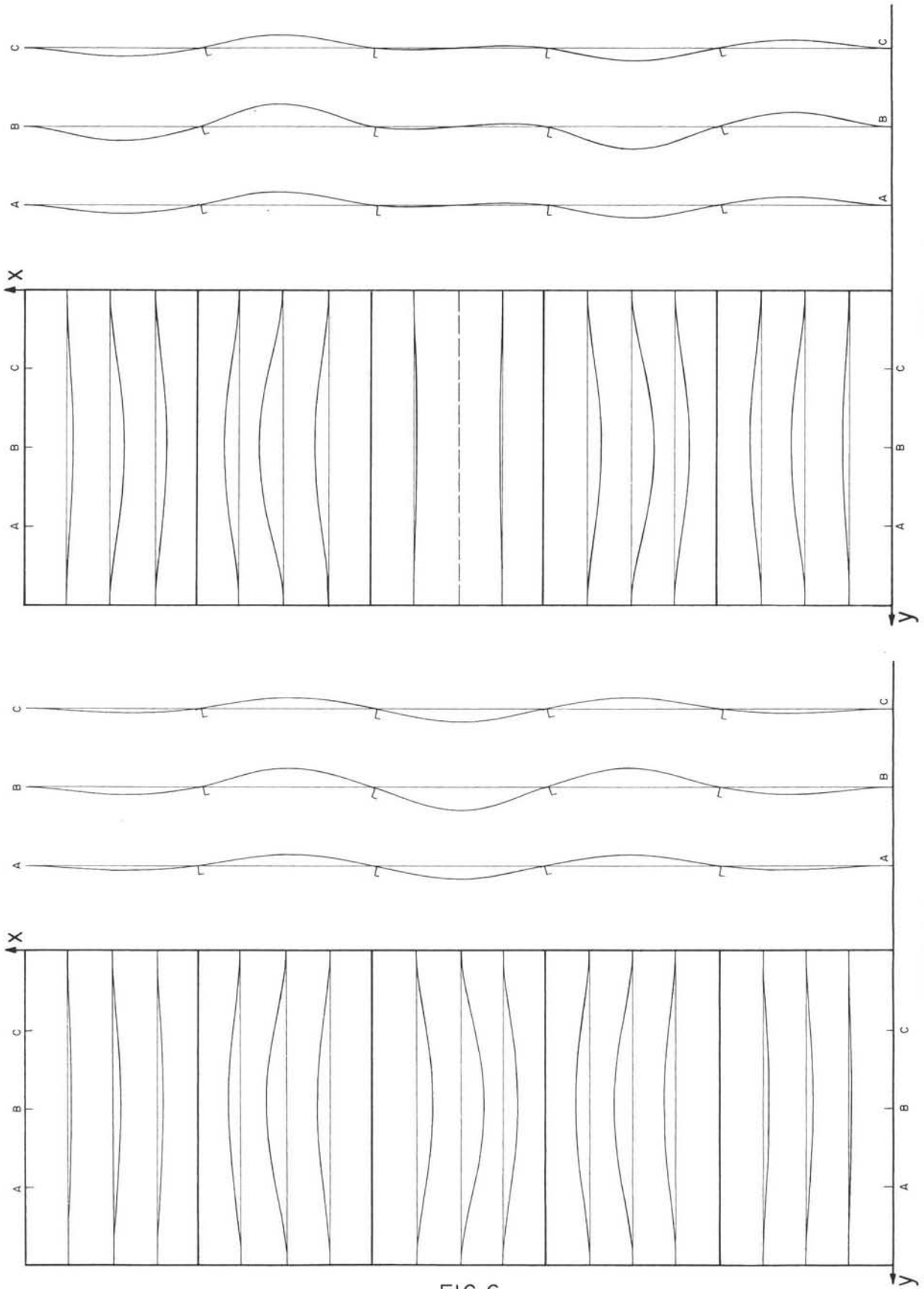


FIG.6

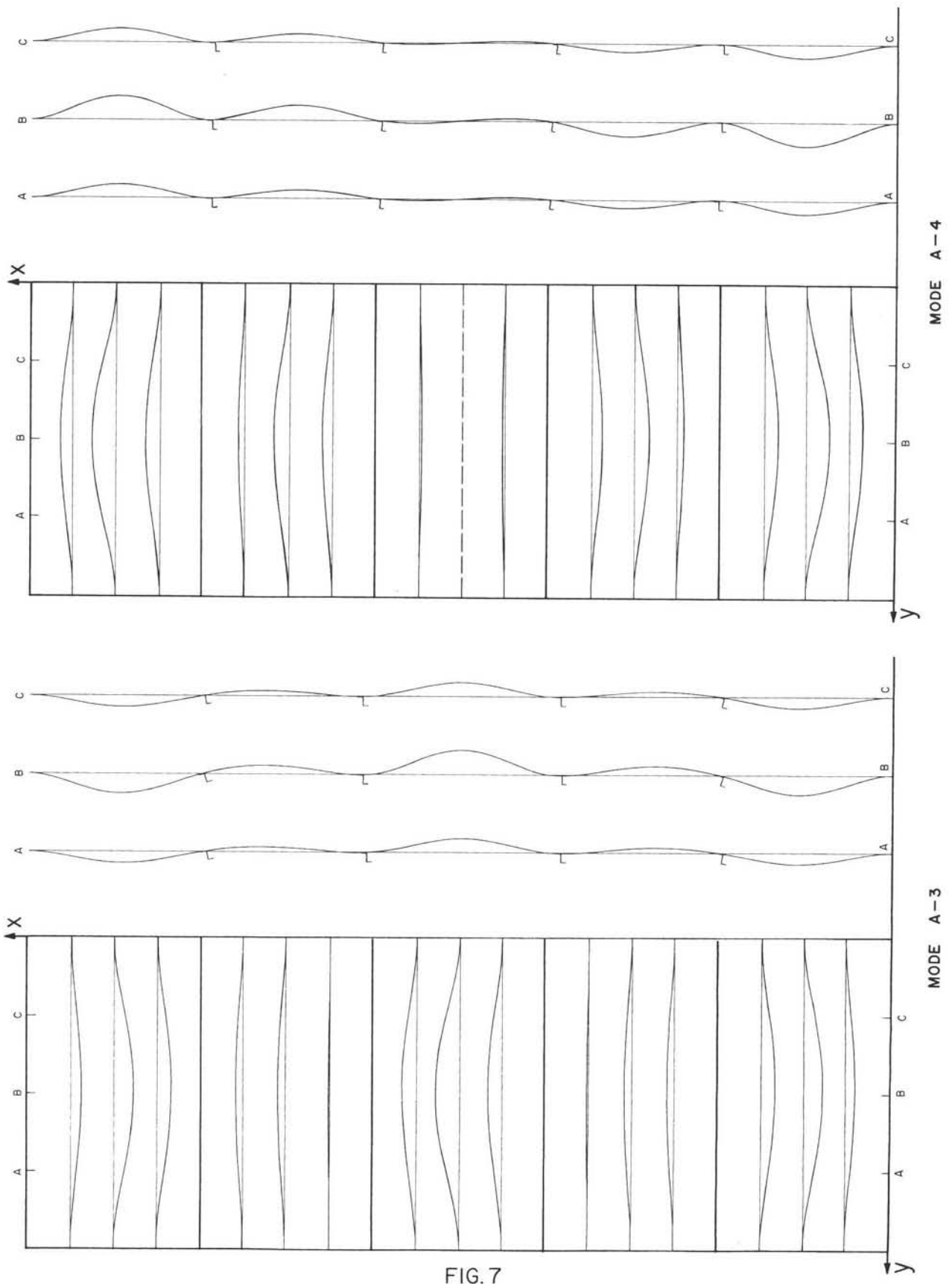


FIG. 7

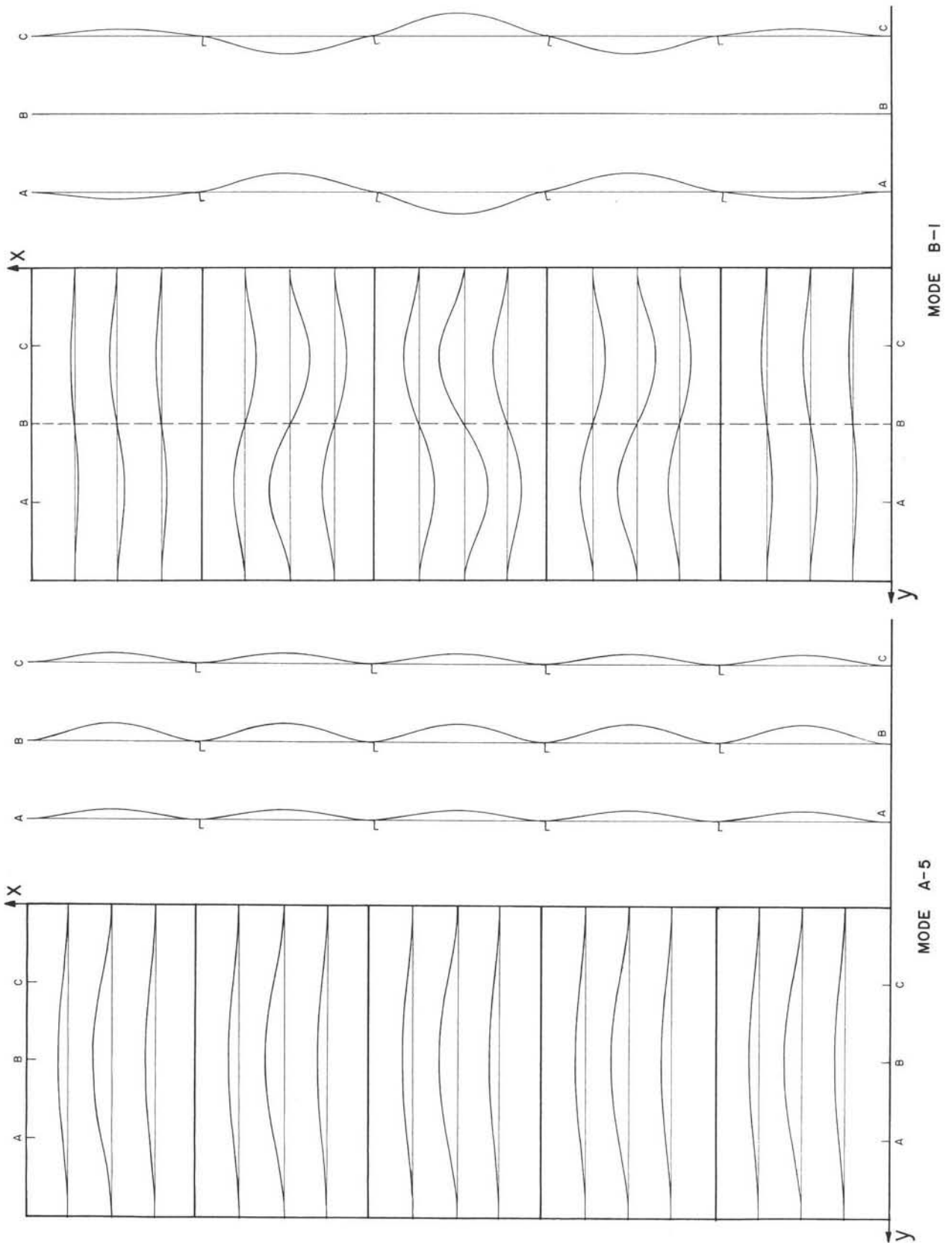


FIG. 8

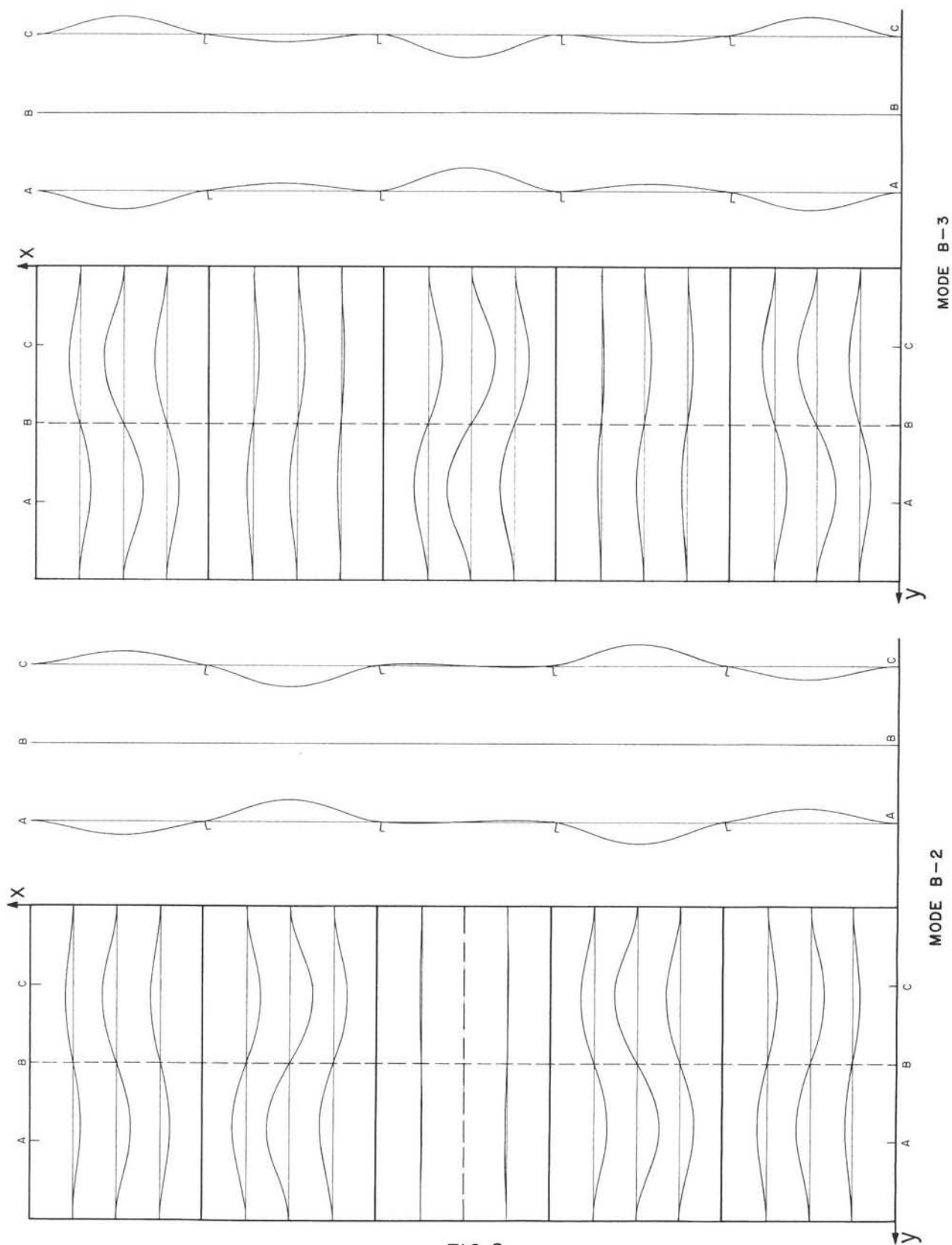


FIG. 9

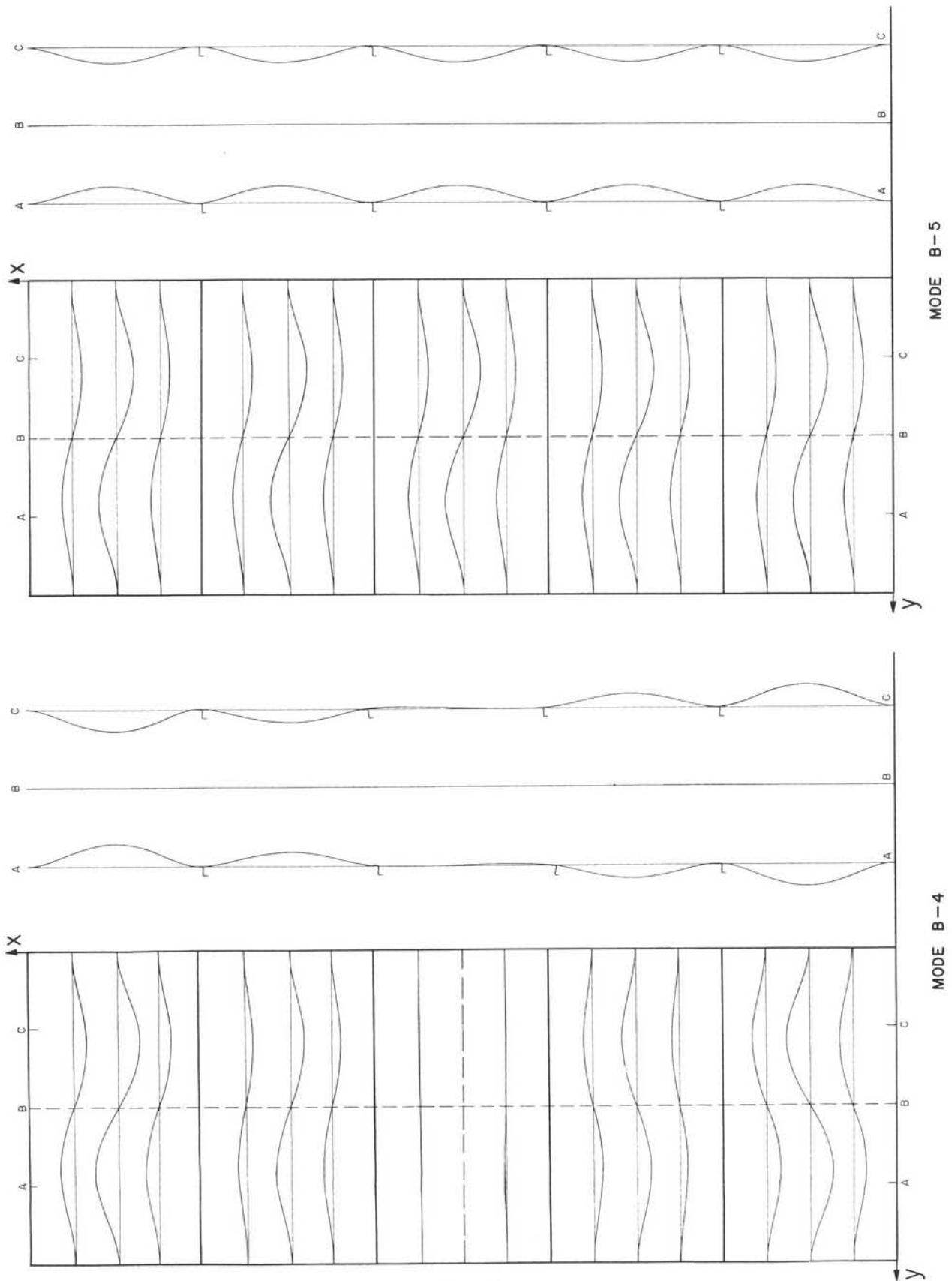


FIG.10

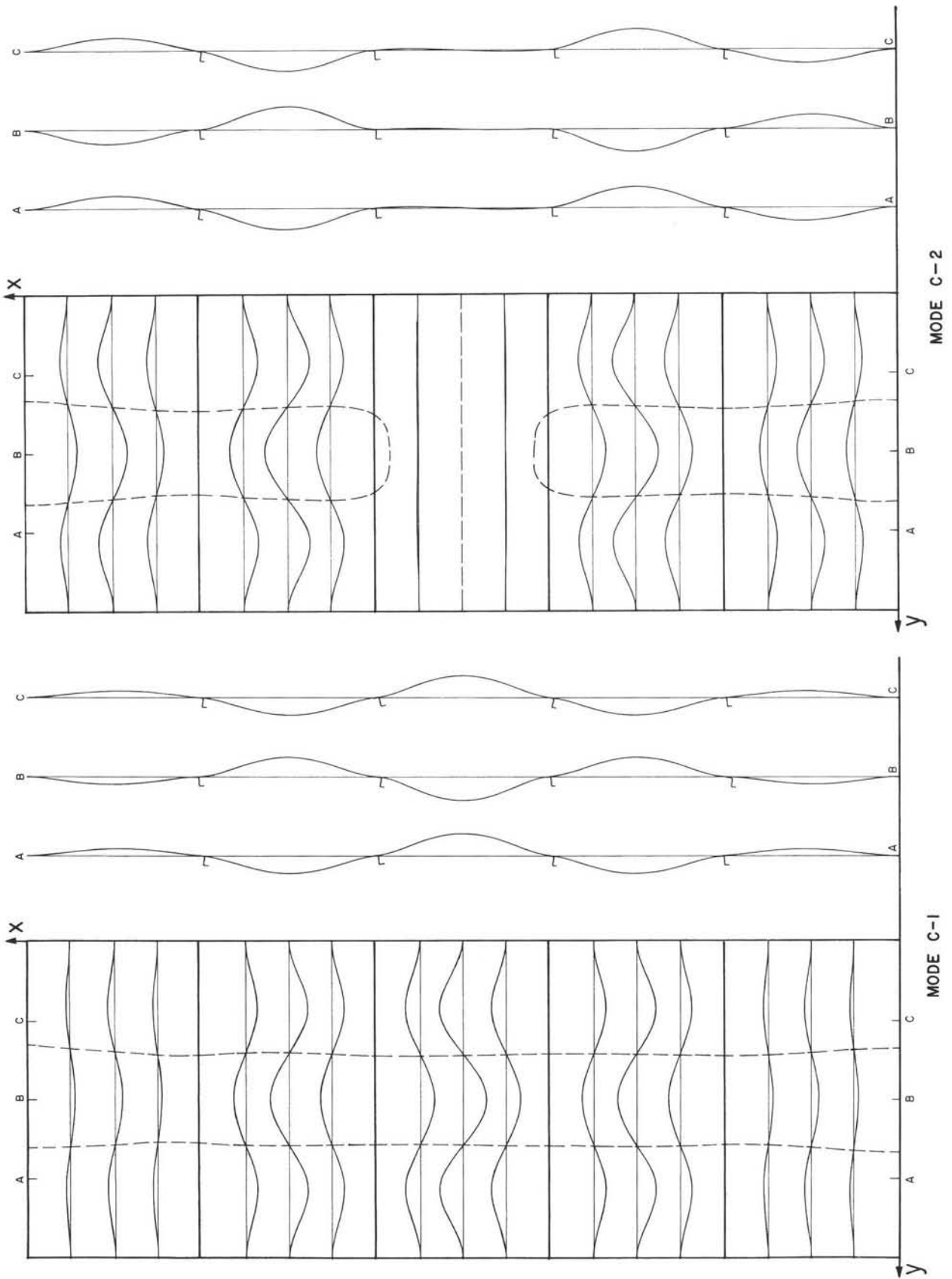


FIG.II

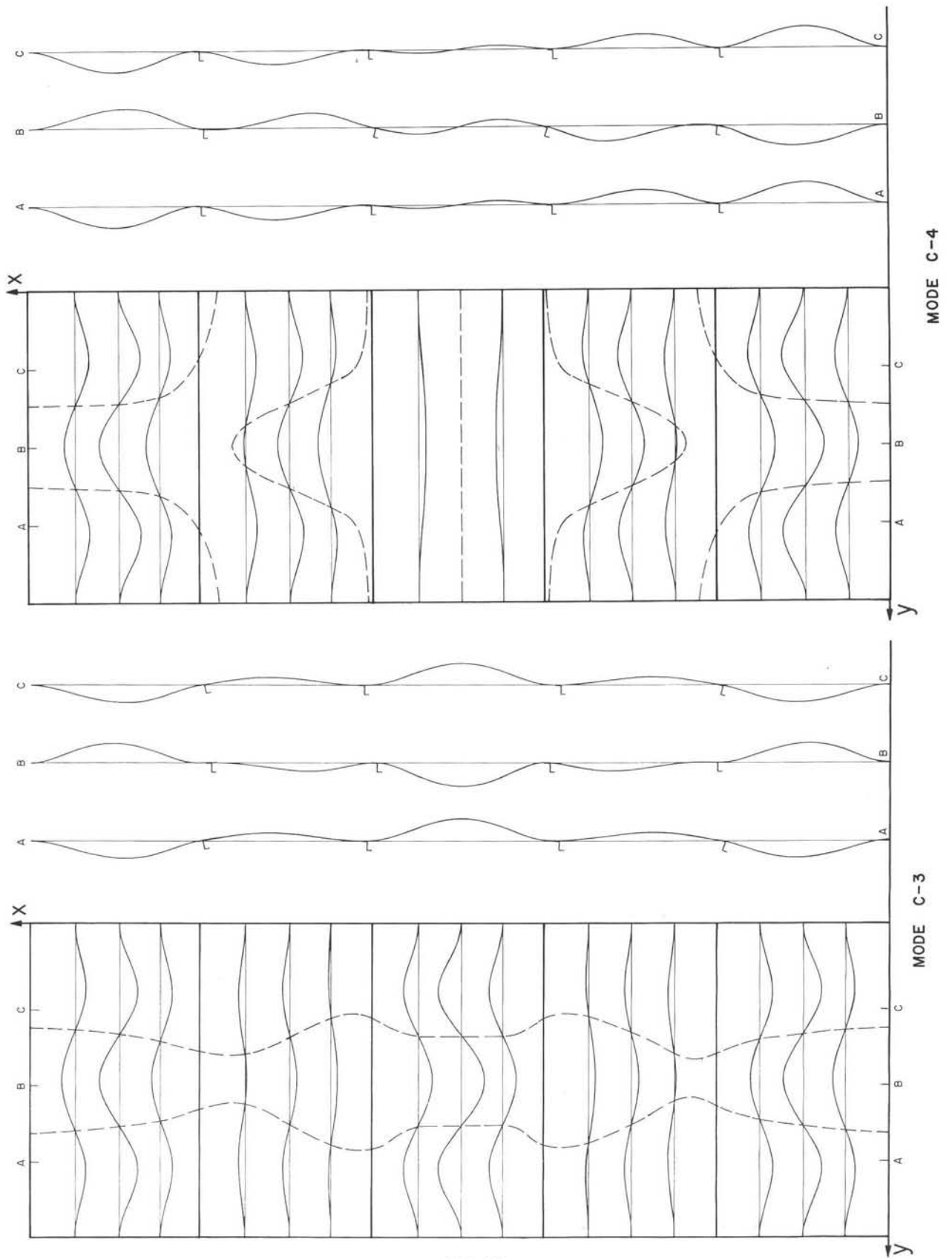


FIG.12

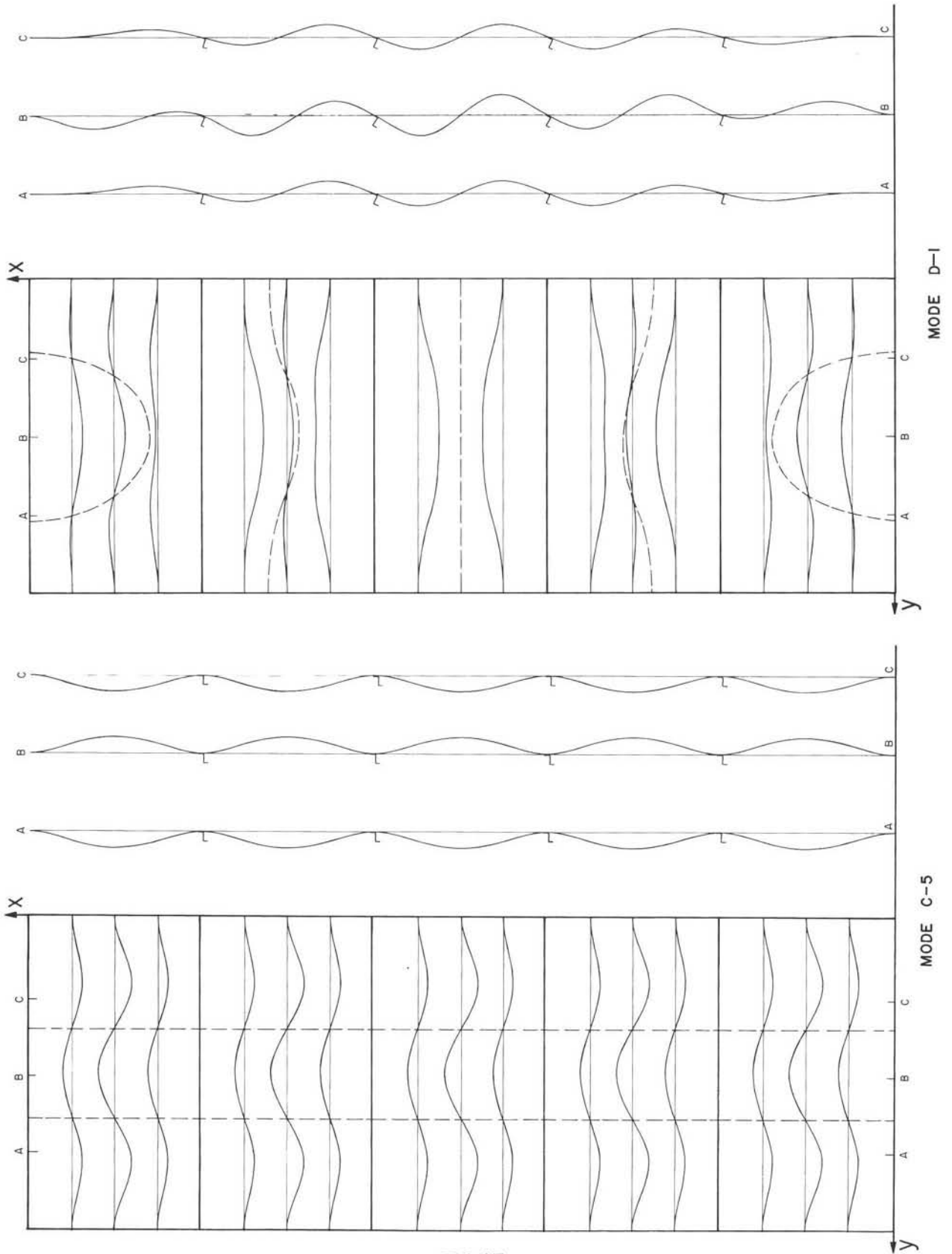


FIG.13

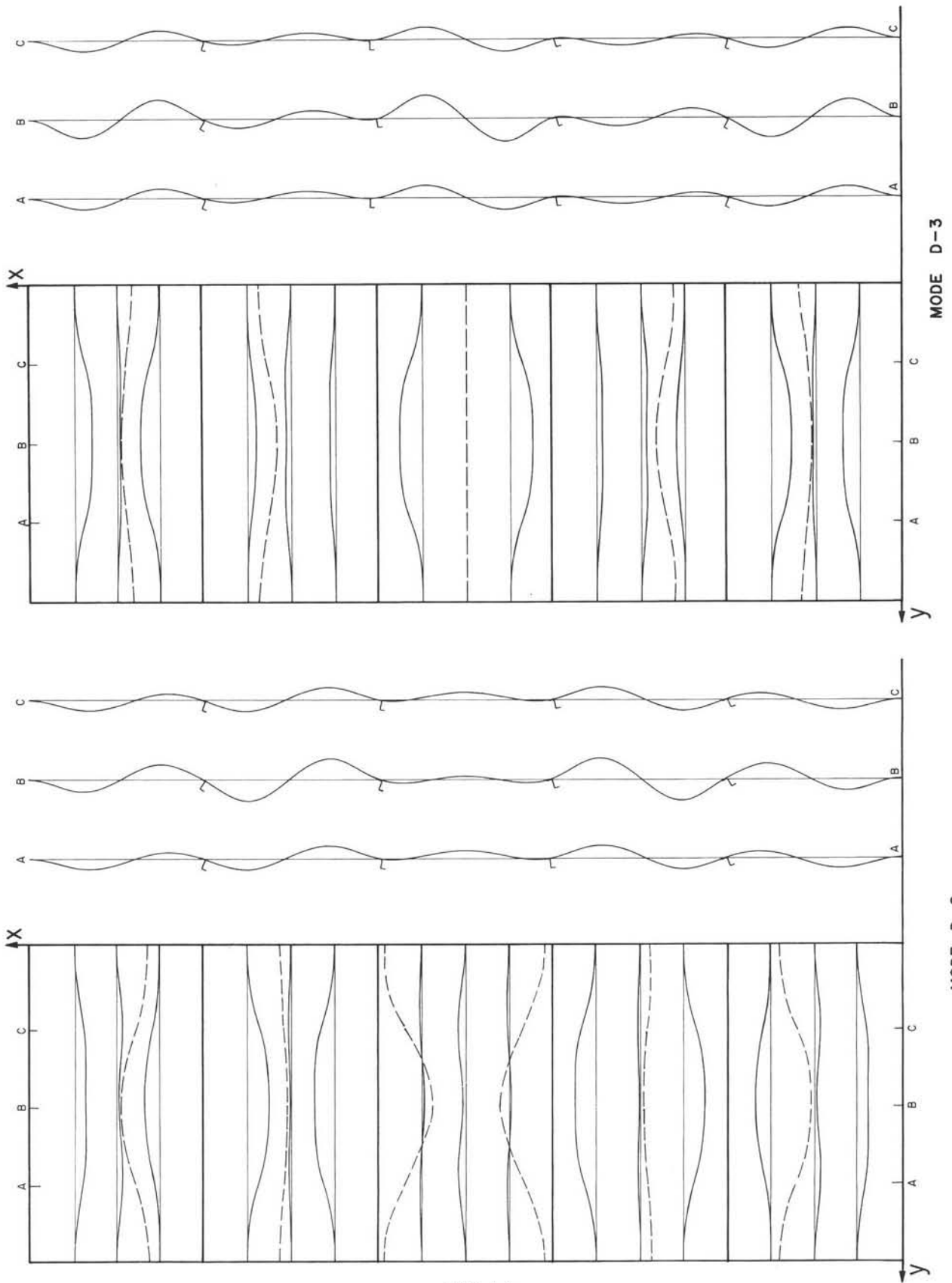


FIG.14

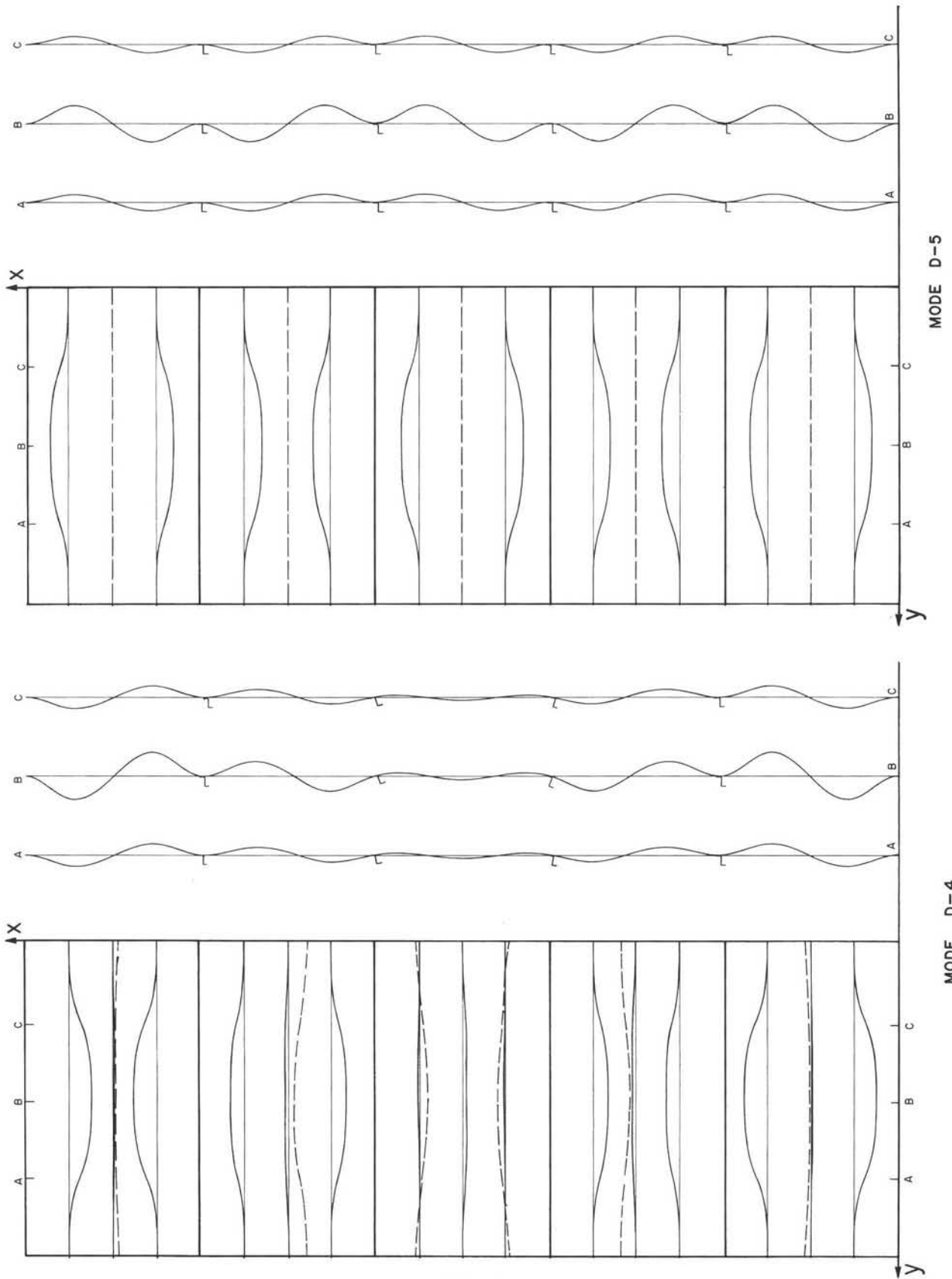


FIG. 15

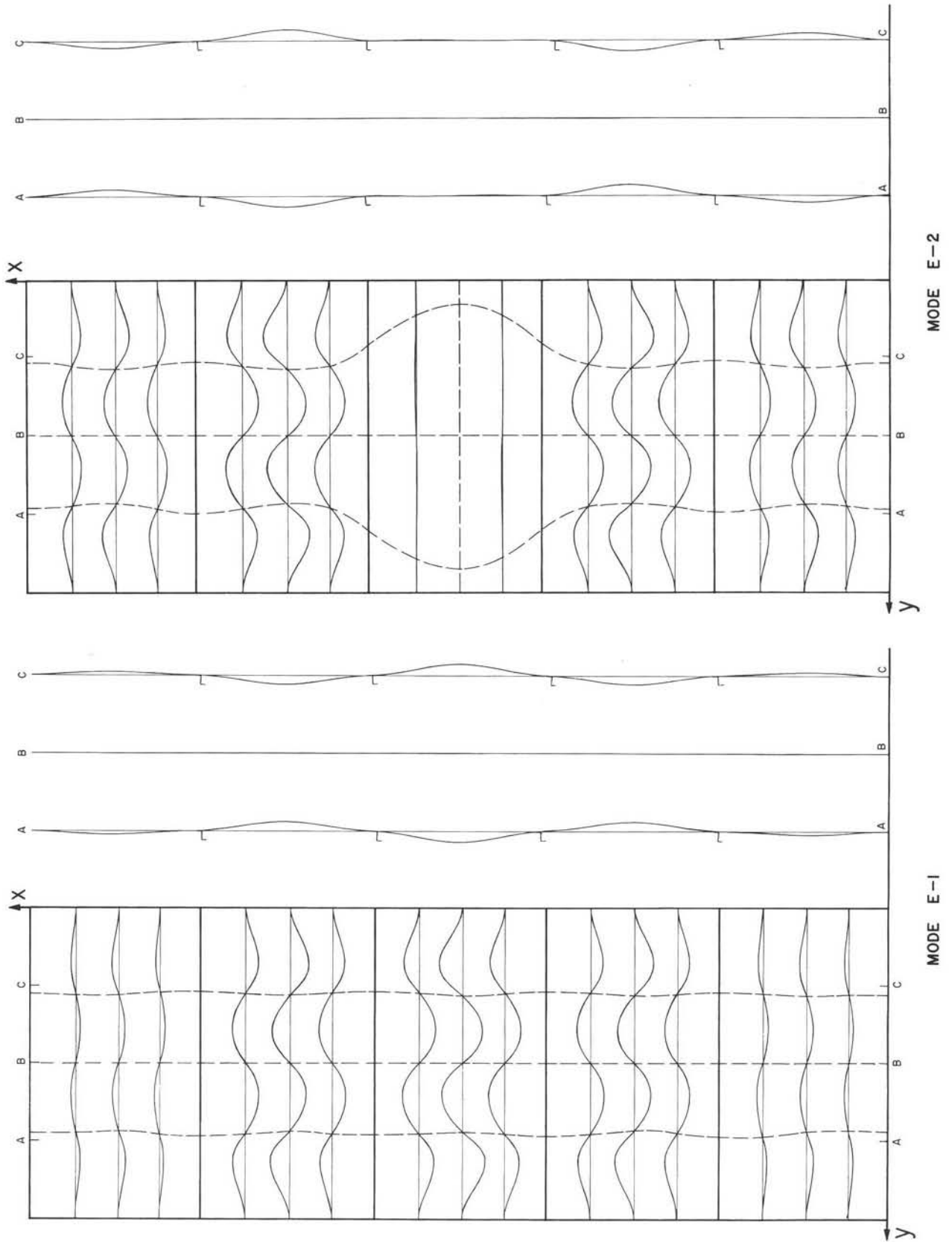


FIG.16

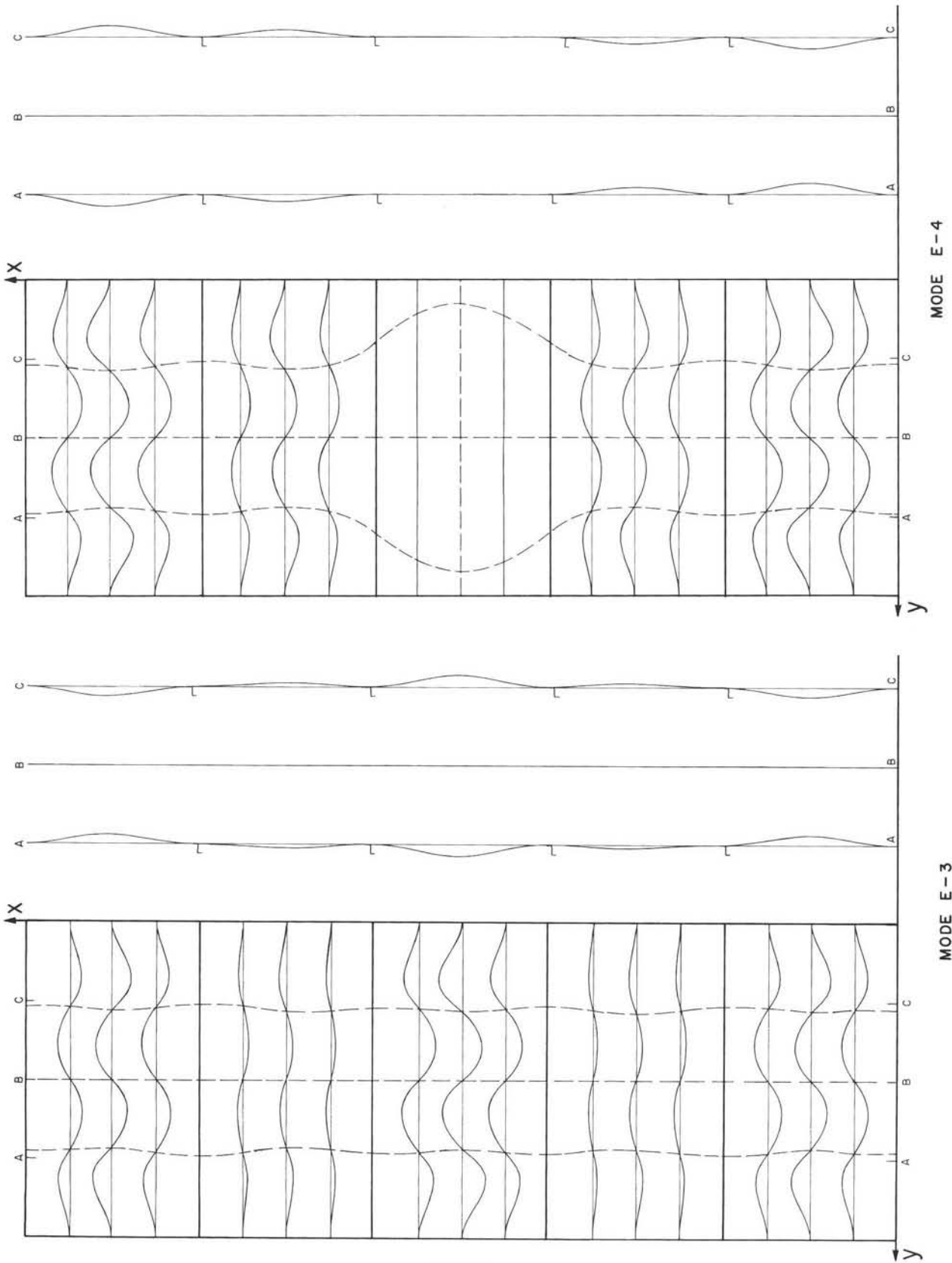


FIG.17

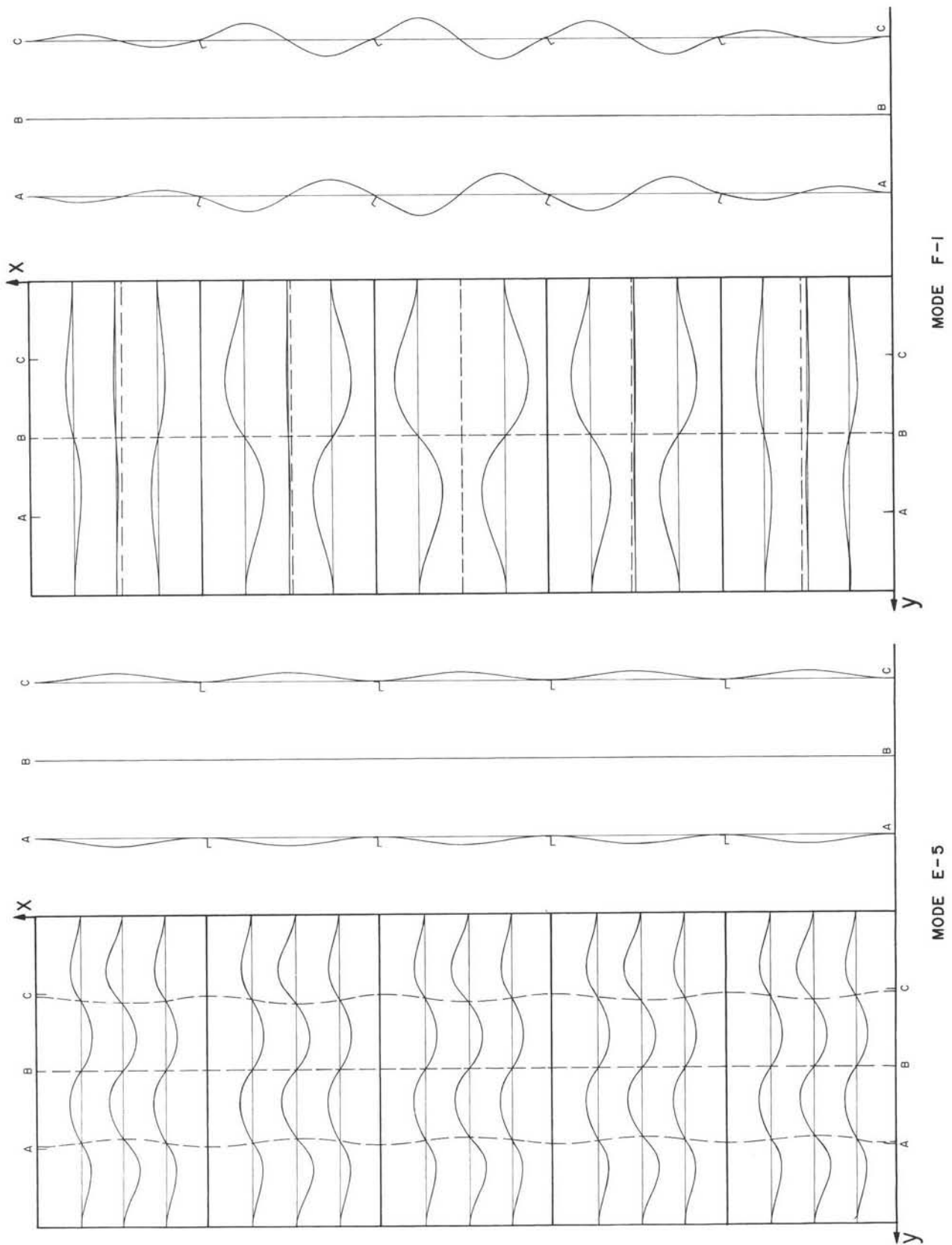


FIG.18

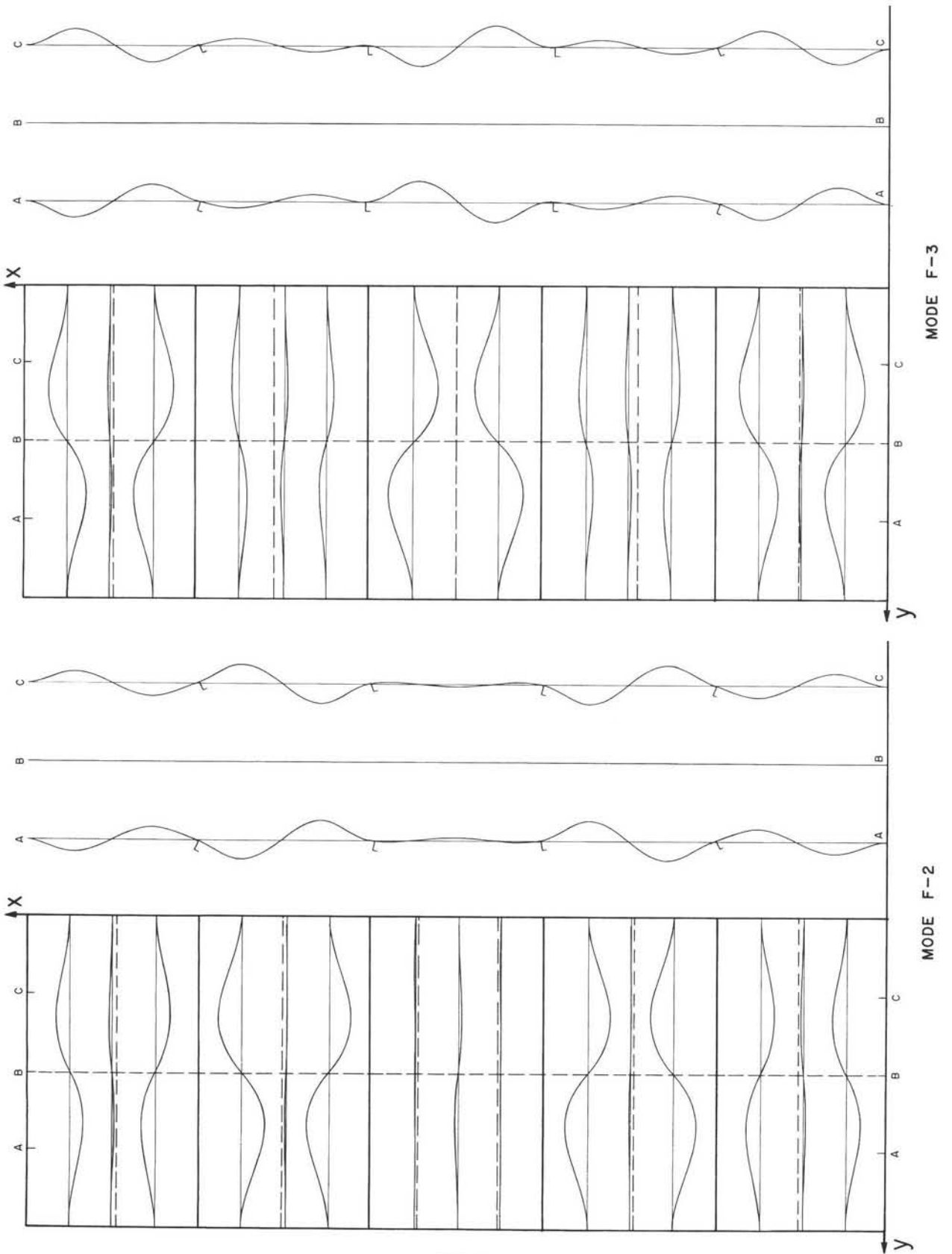


FIG.19

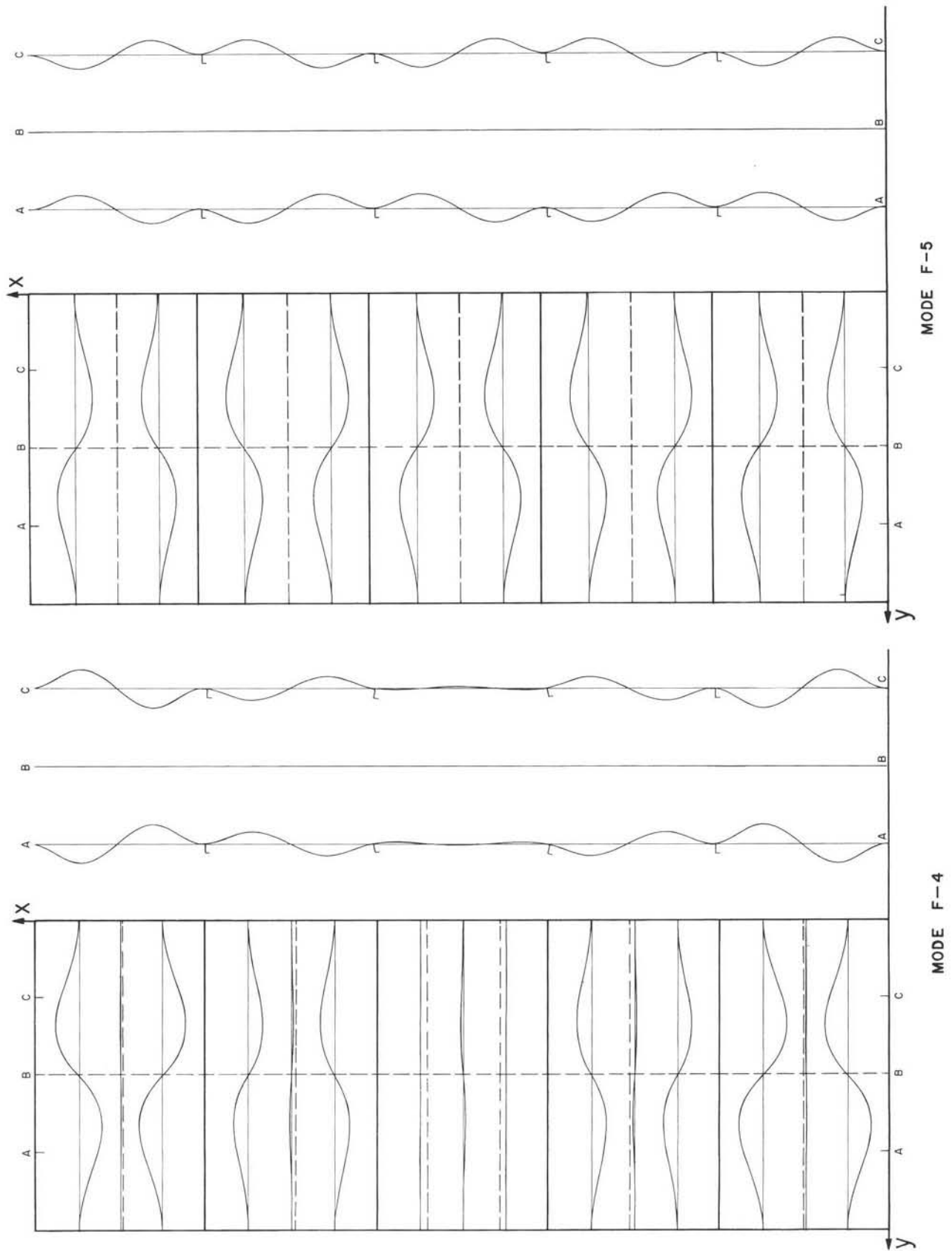


FIG. 20

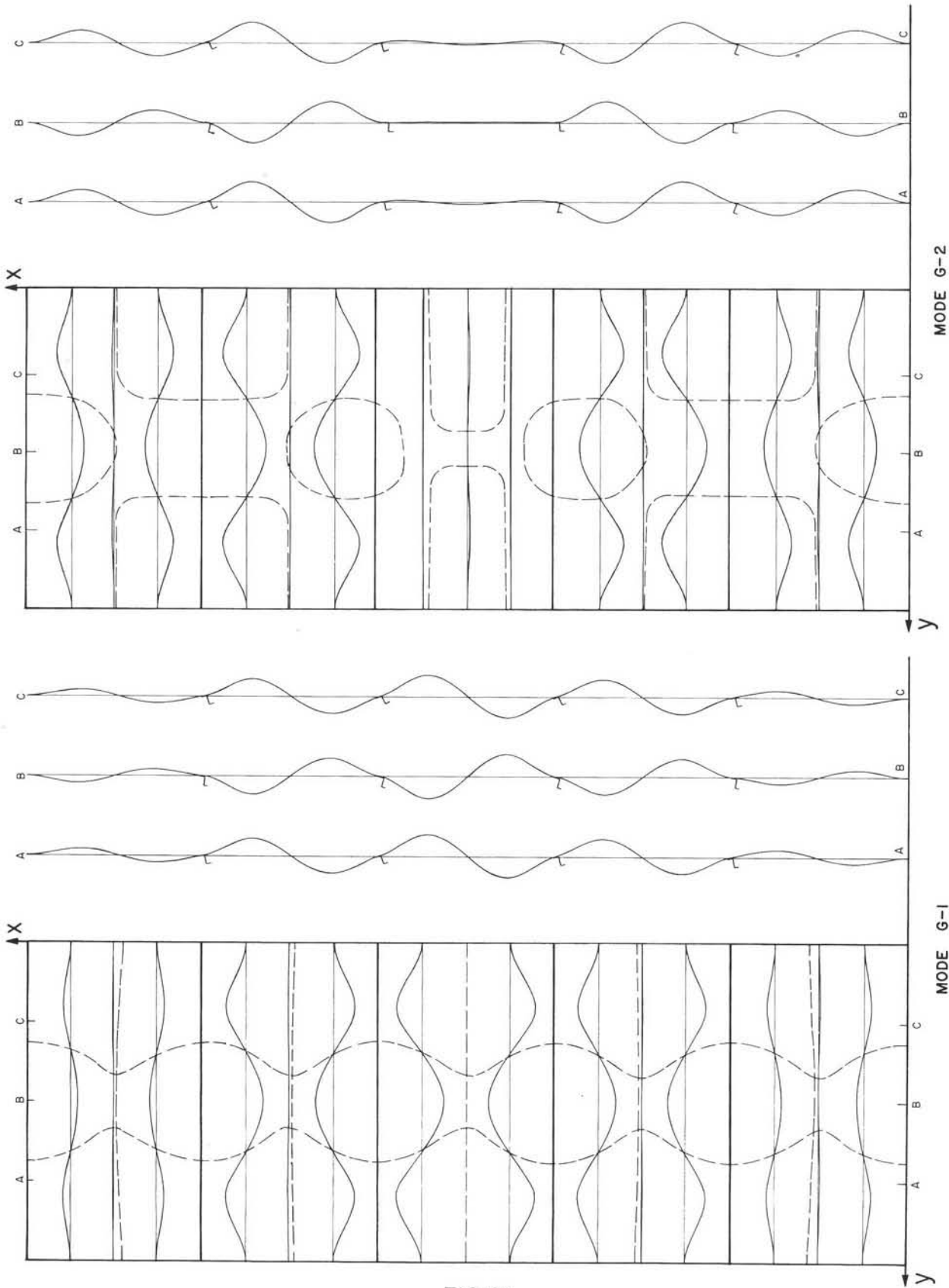


FIG. 21

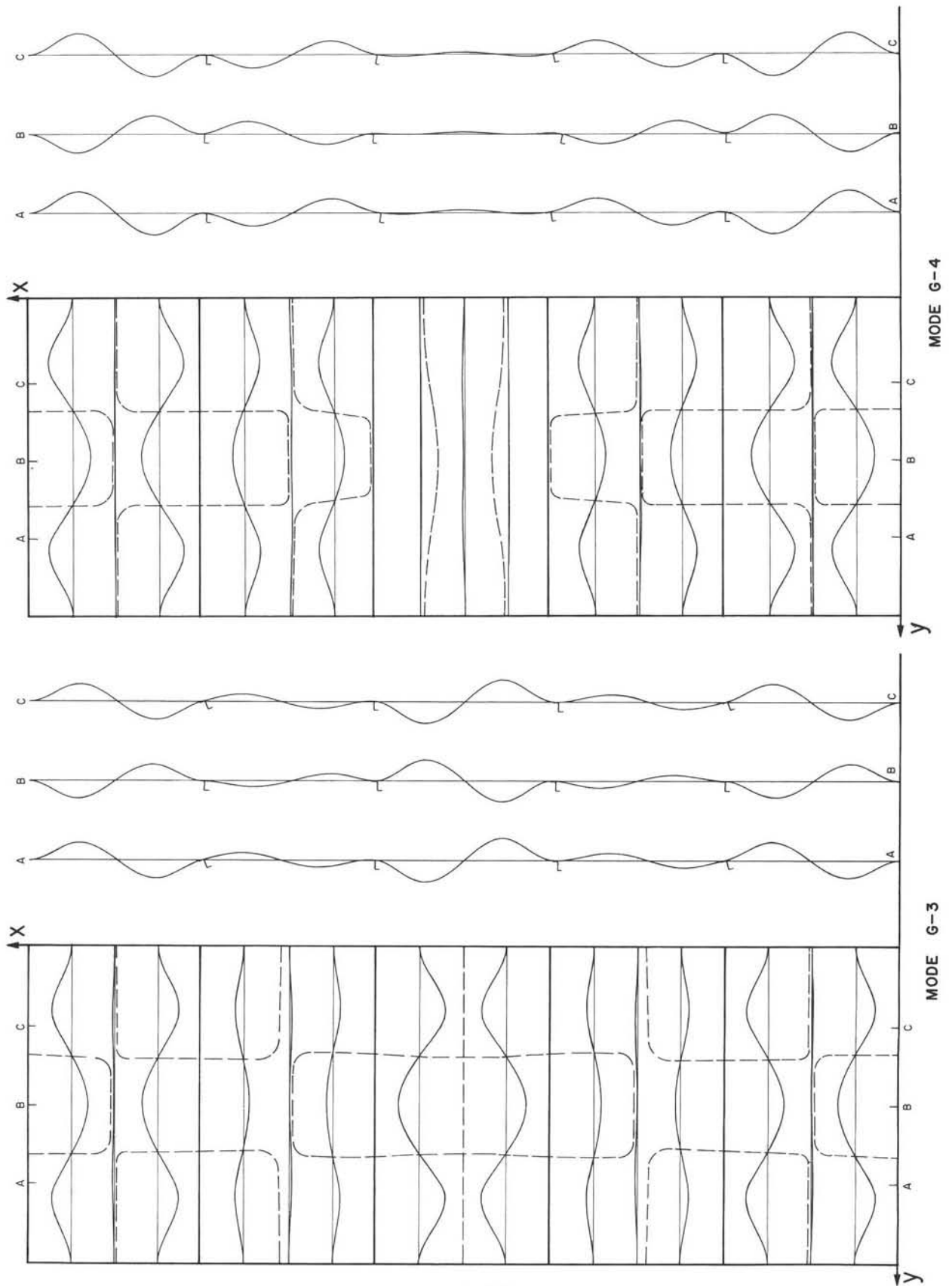


FIG. 22

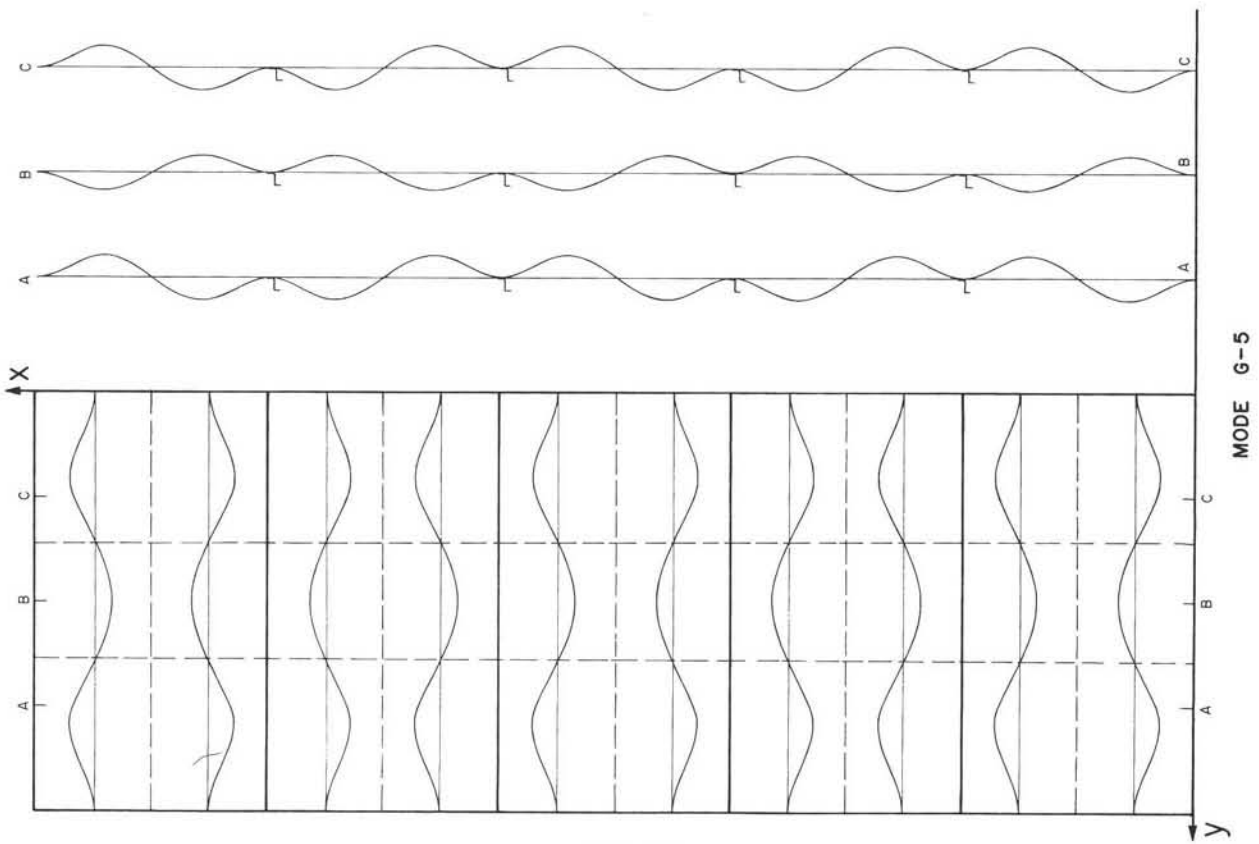
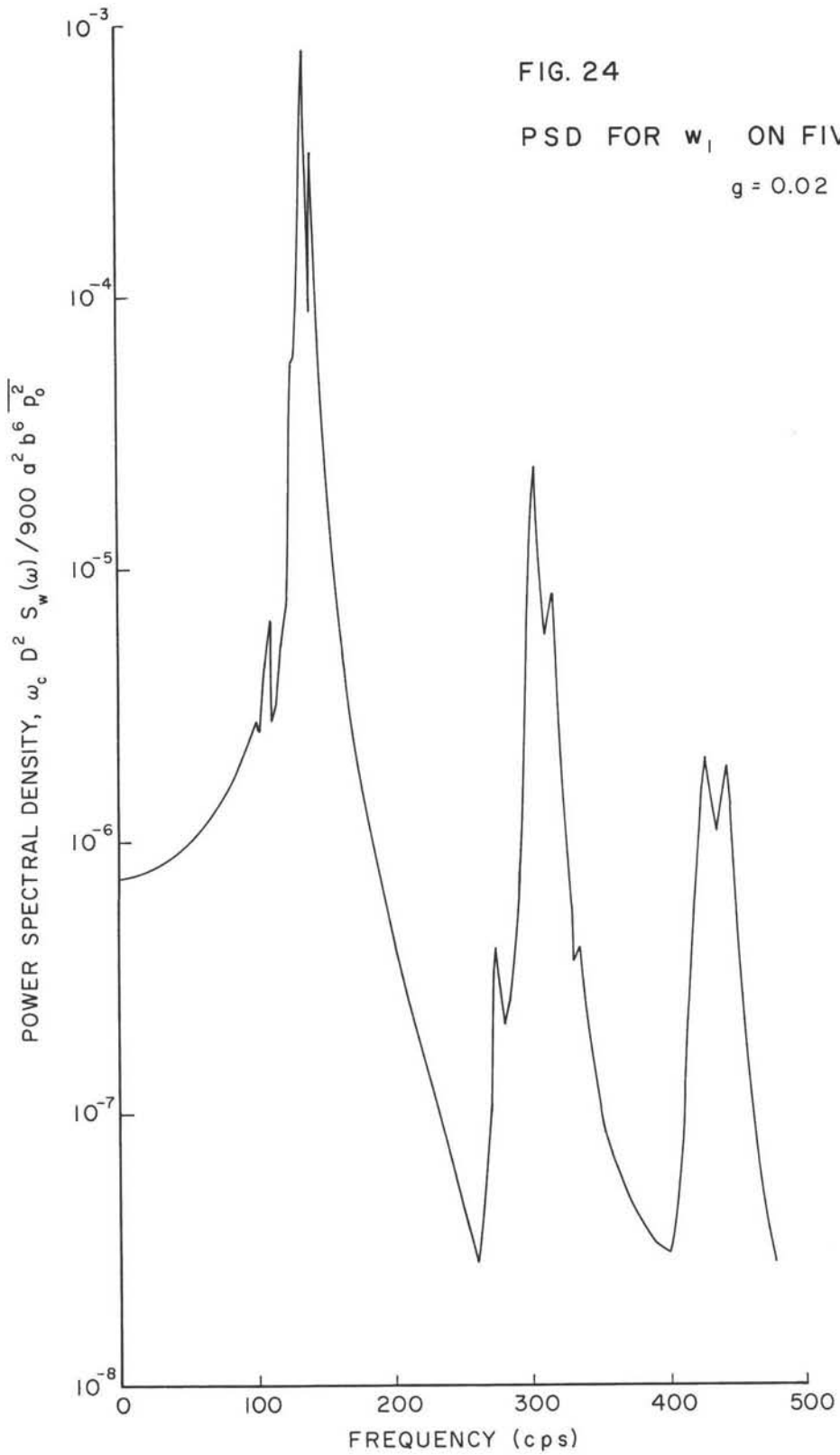
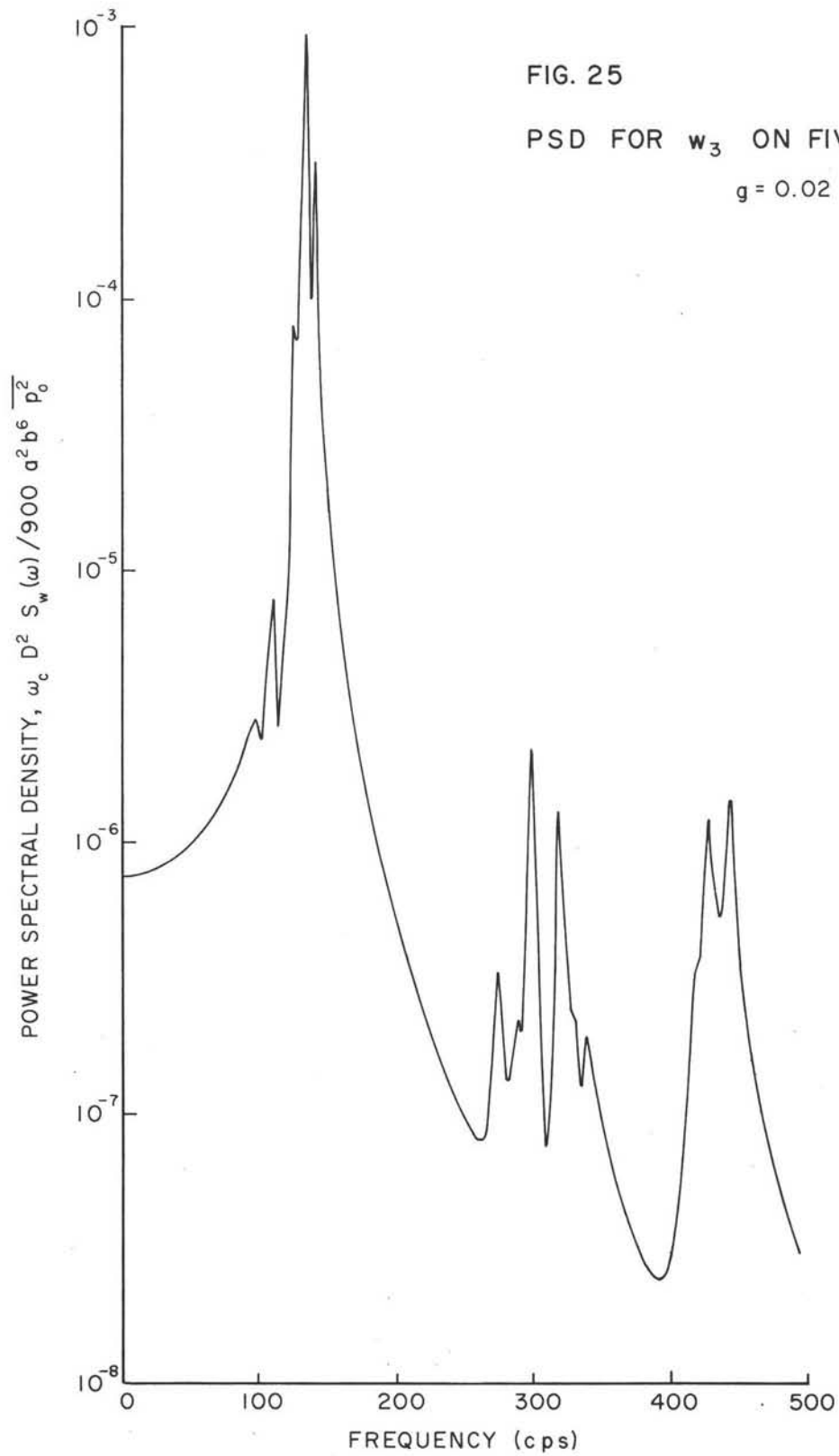
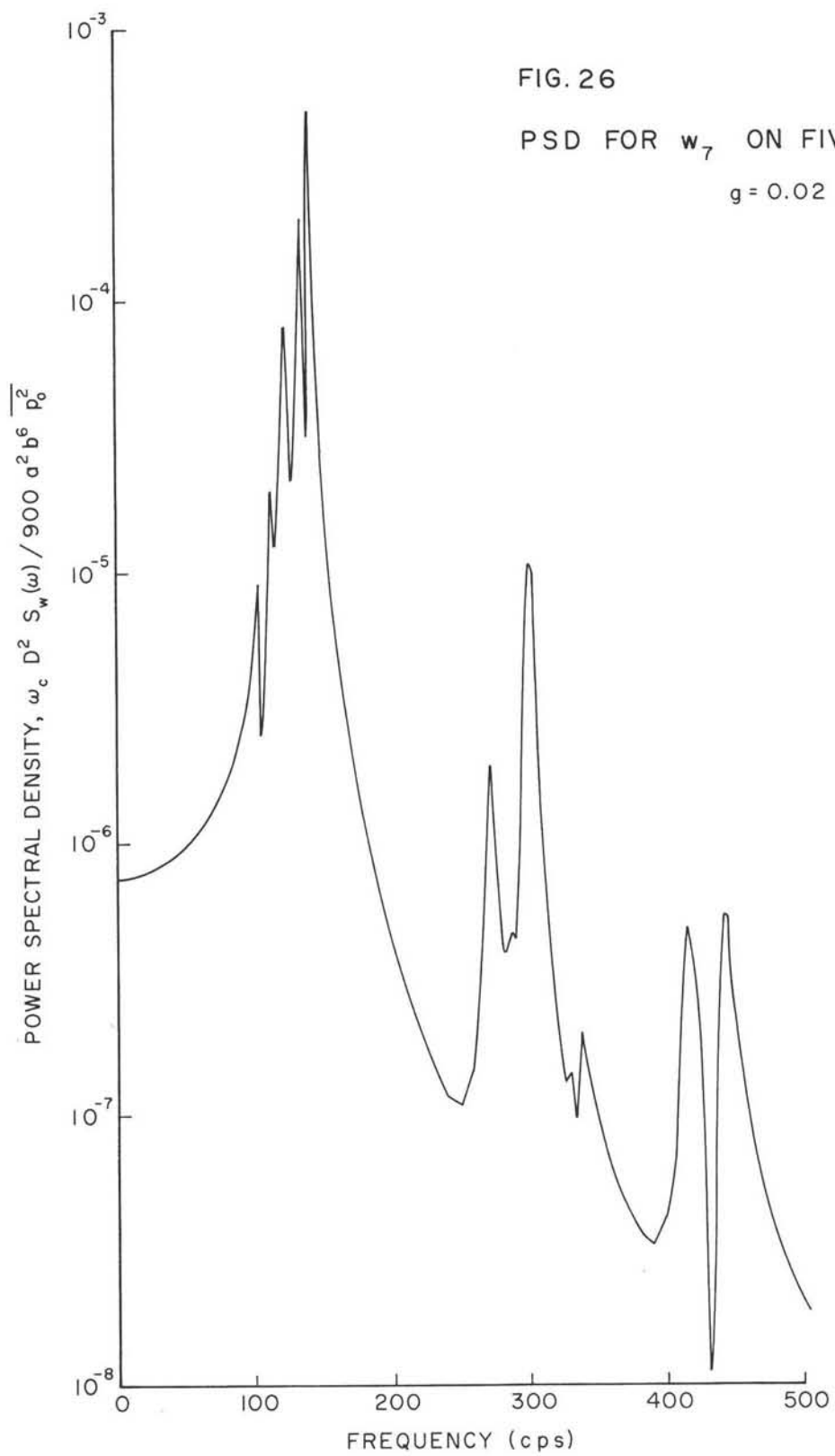
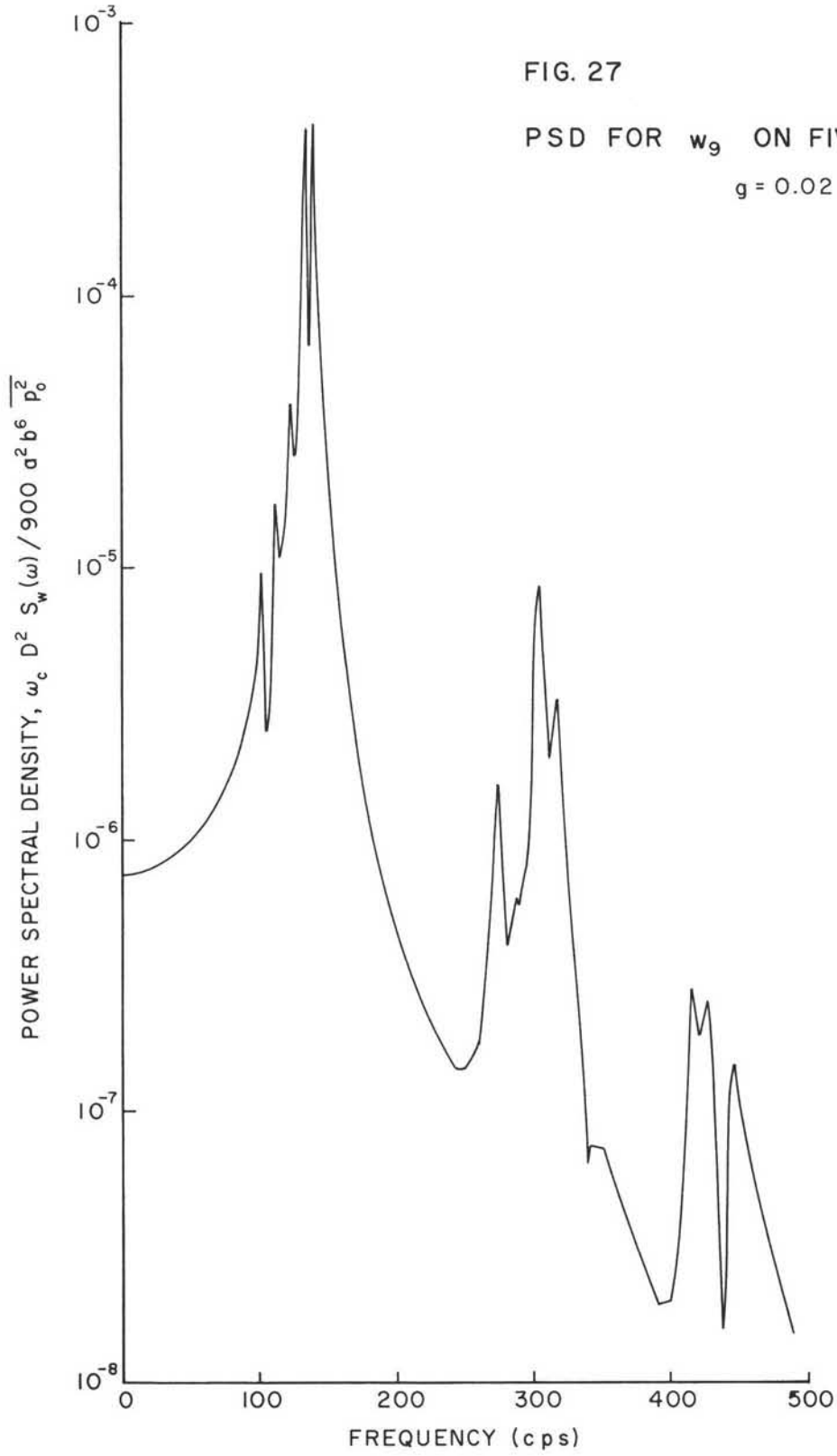


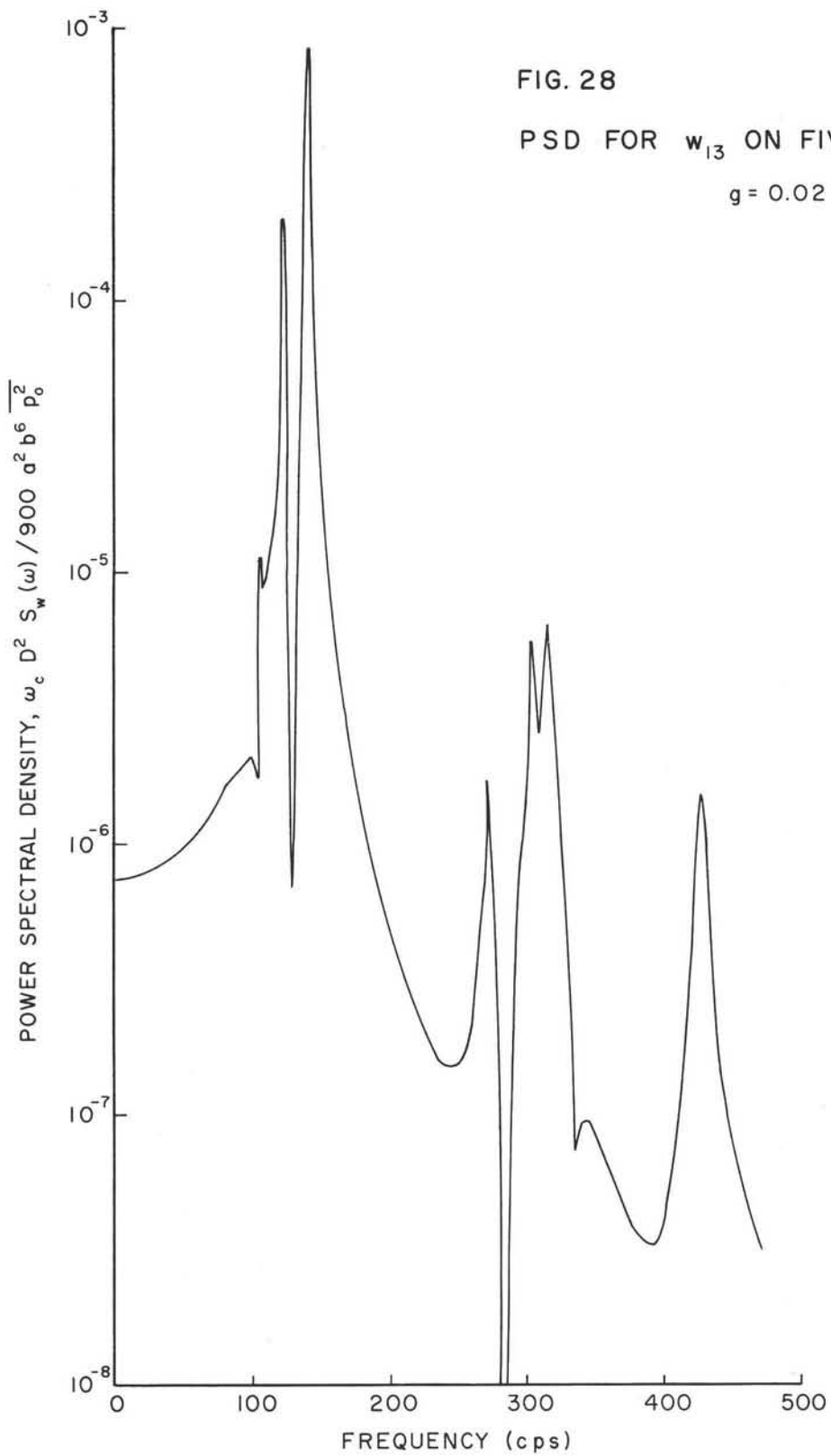
FIG. 23

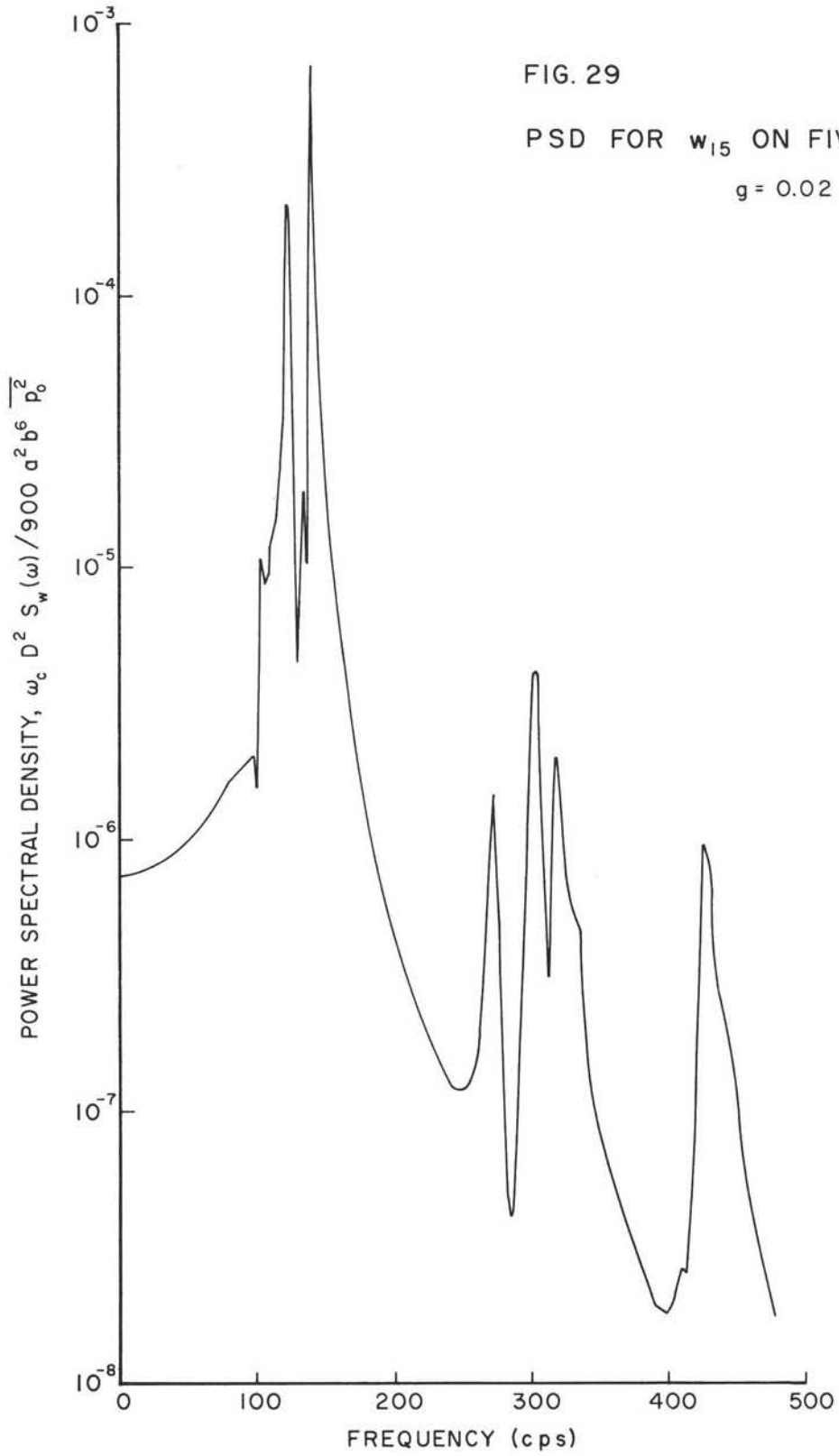


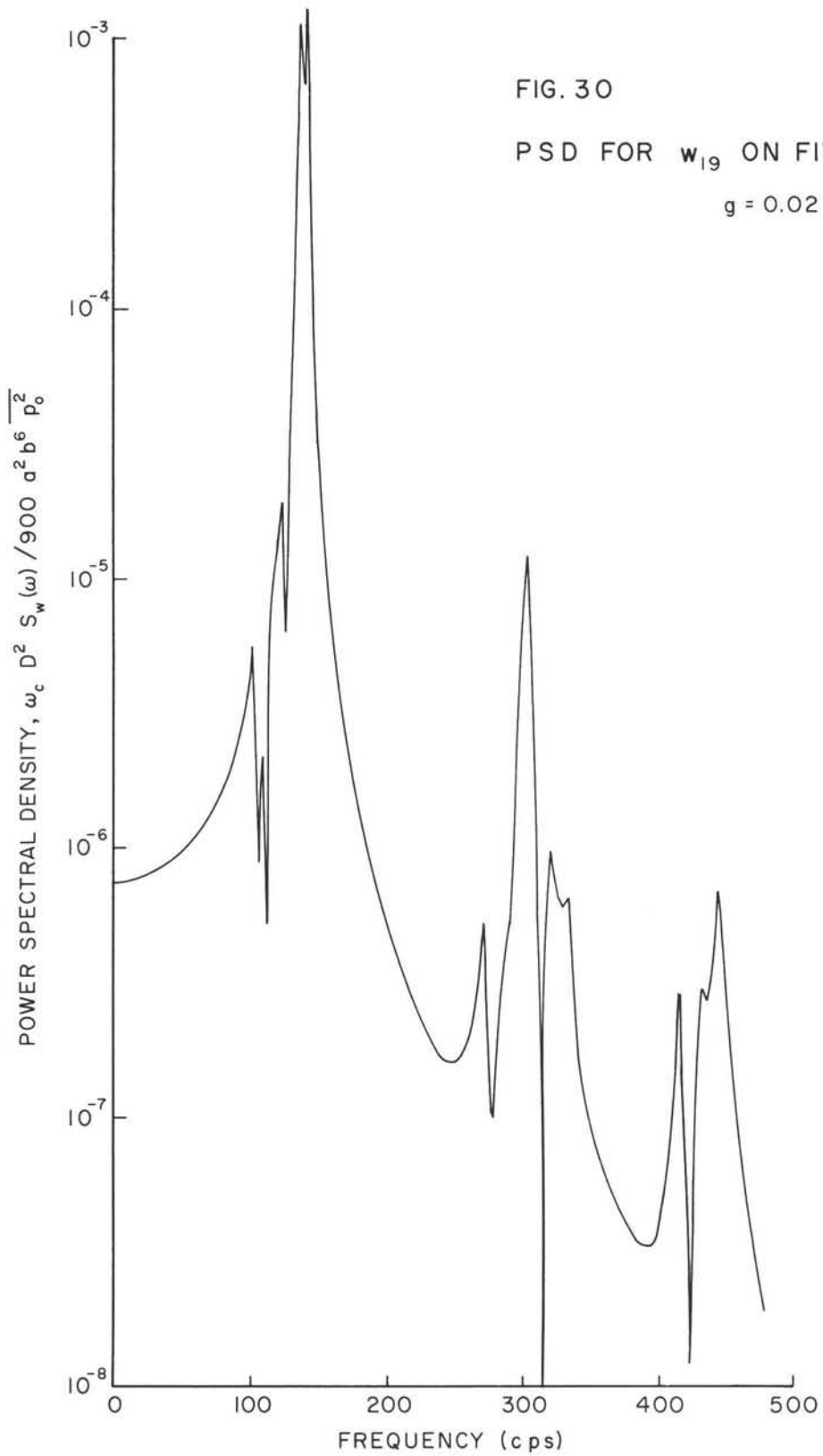


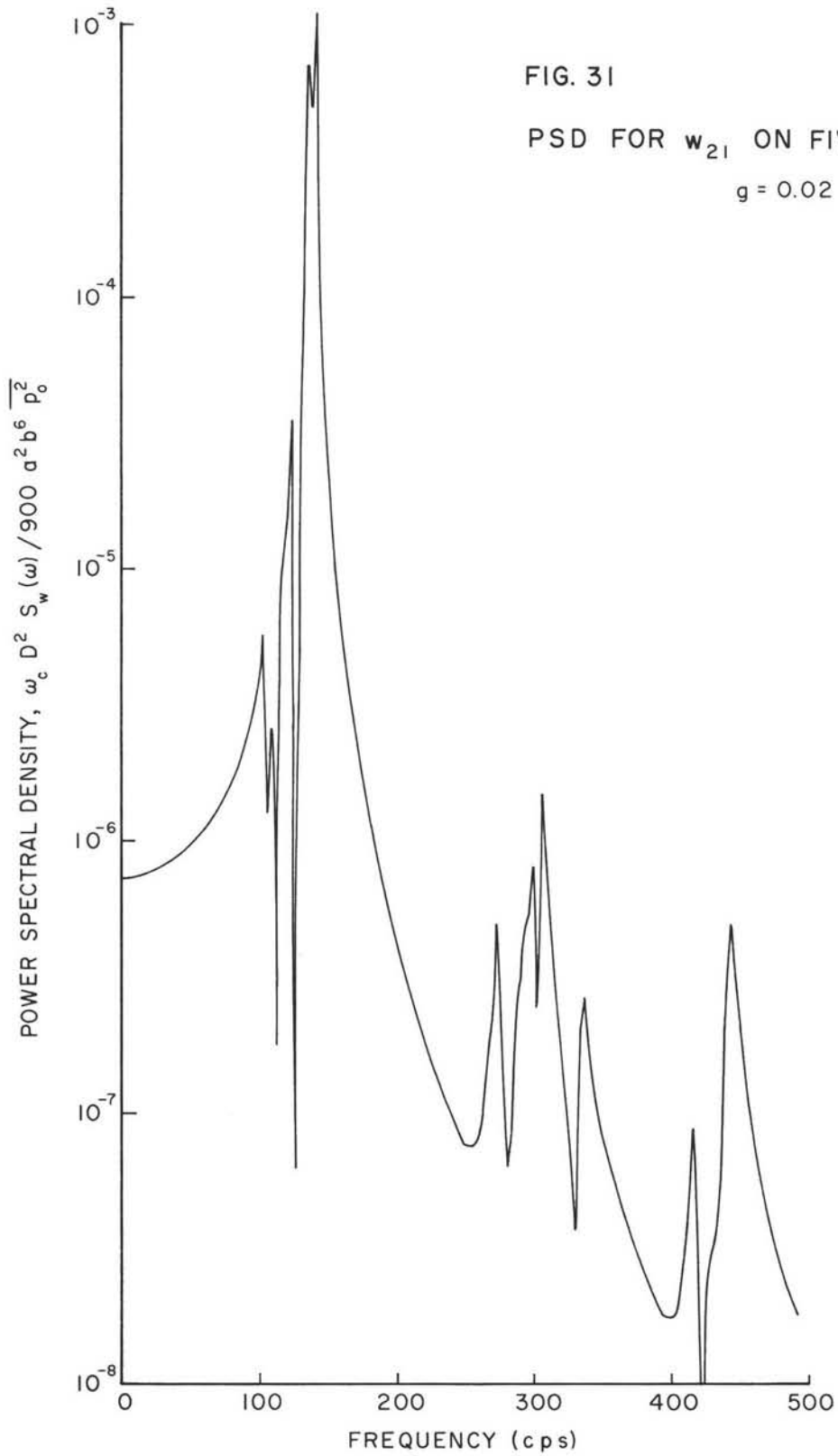












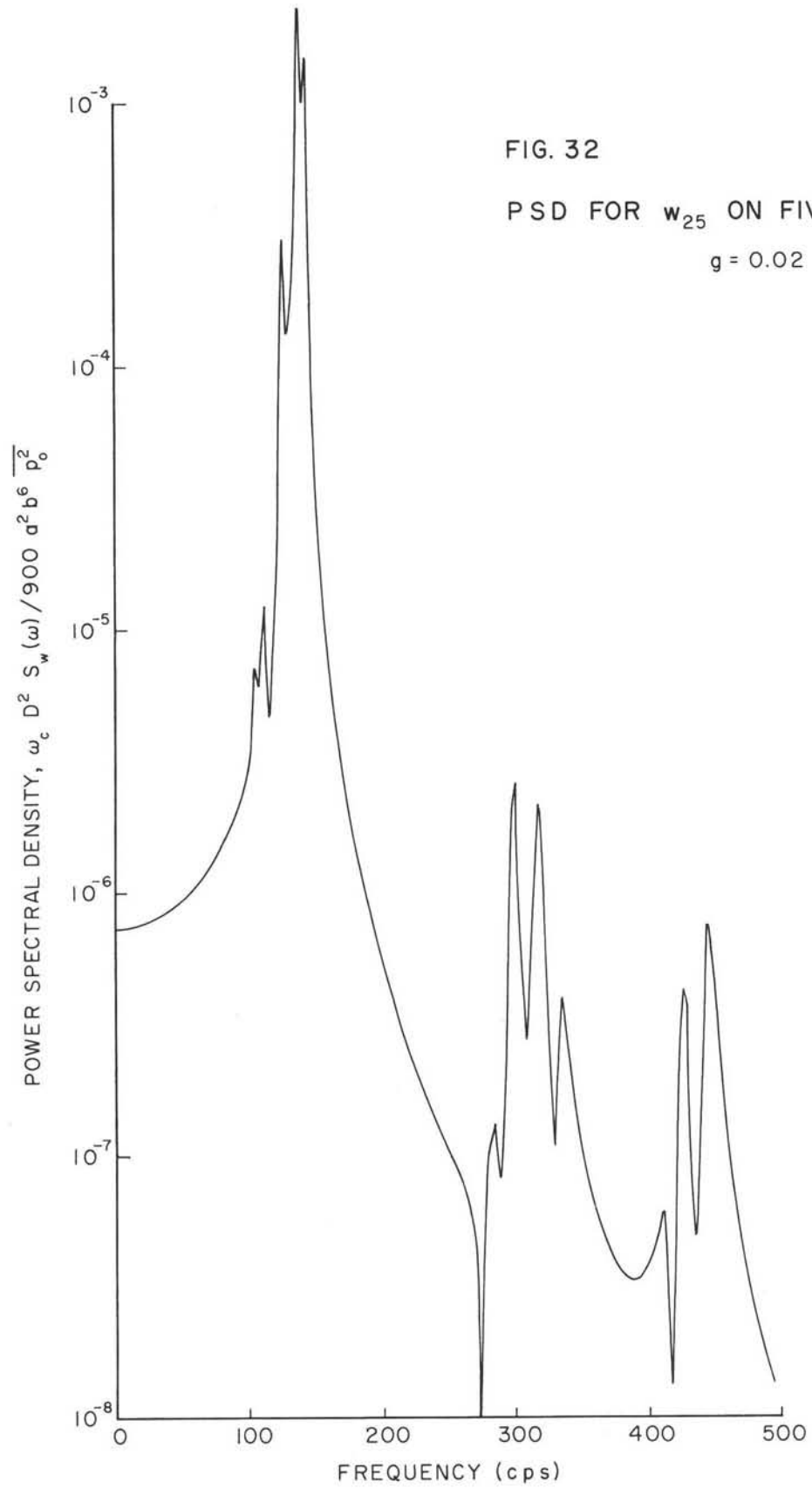


FIG. 32

PSD FOR w_{25} ON FIVE-BAY PANEL

$g = 0.02$

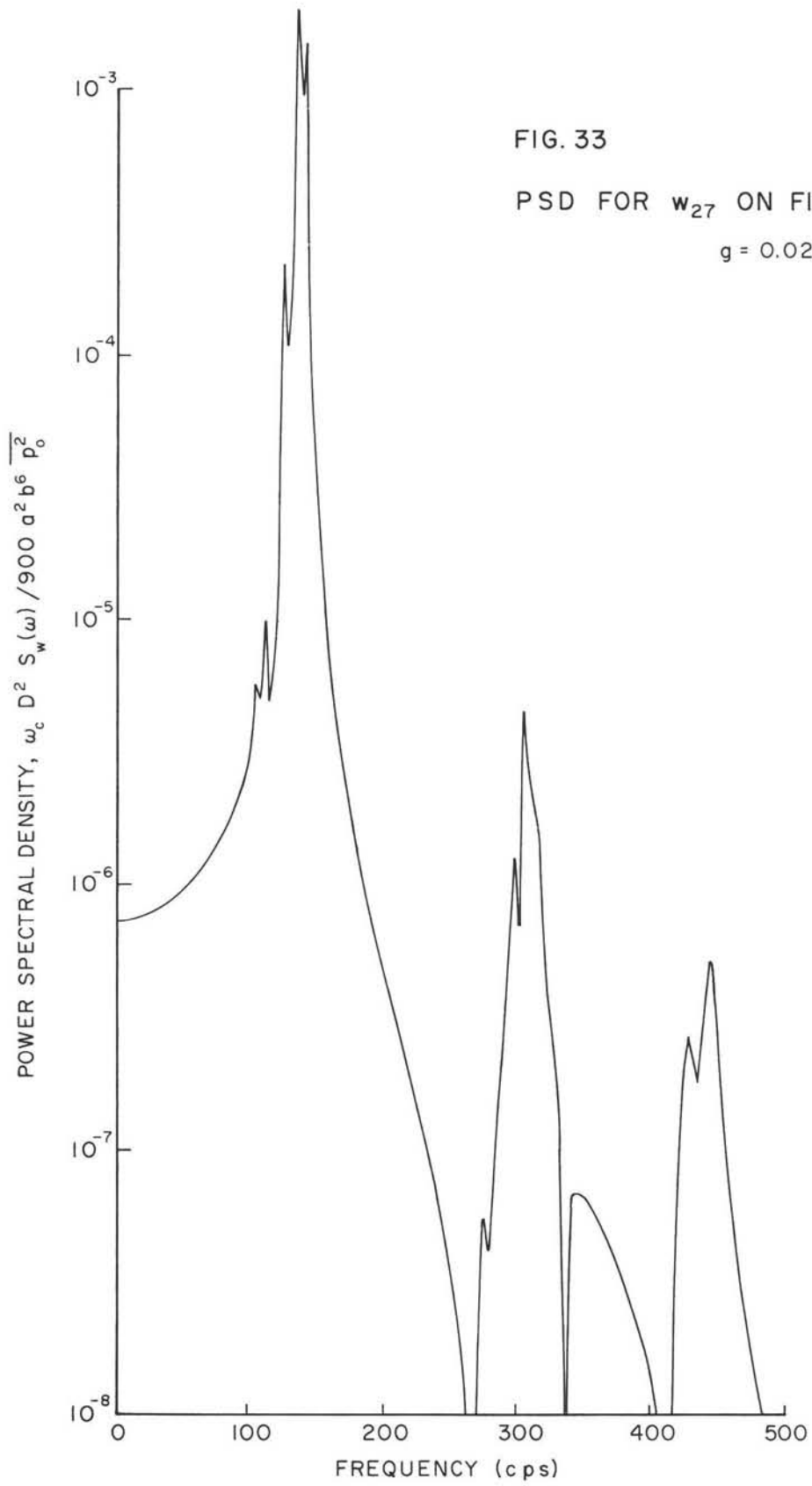


FIG. 33

PSD FOR w_{27} ON FIVE-BAY PANEL

$g = 0.02$

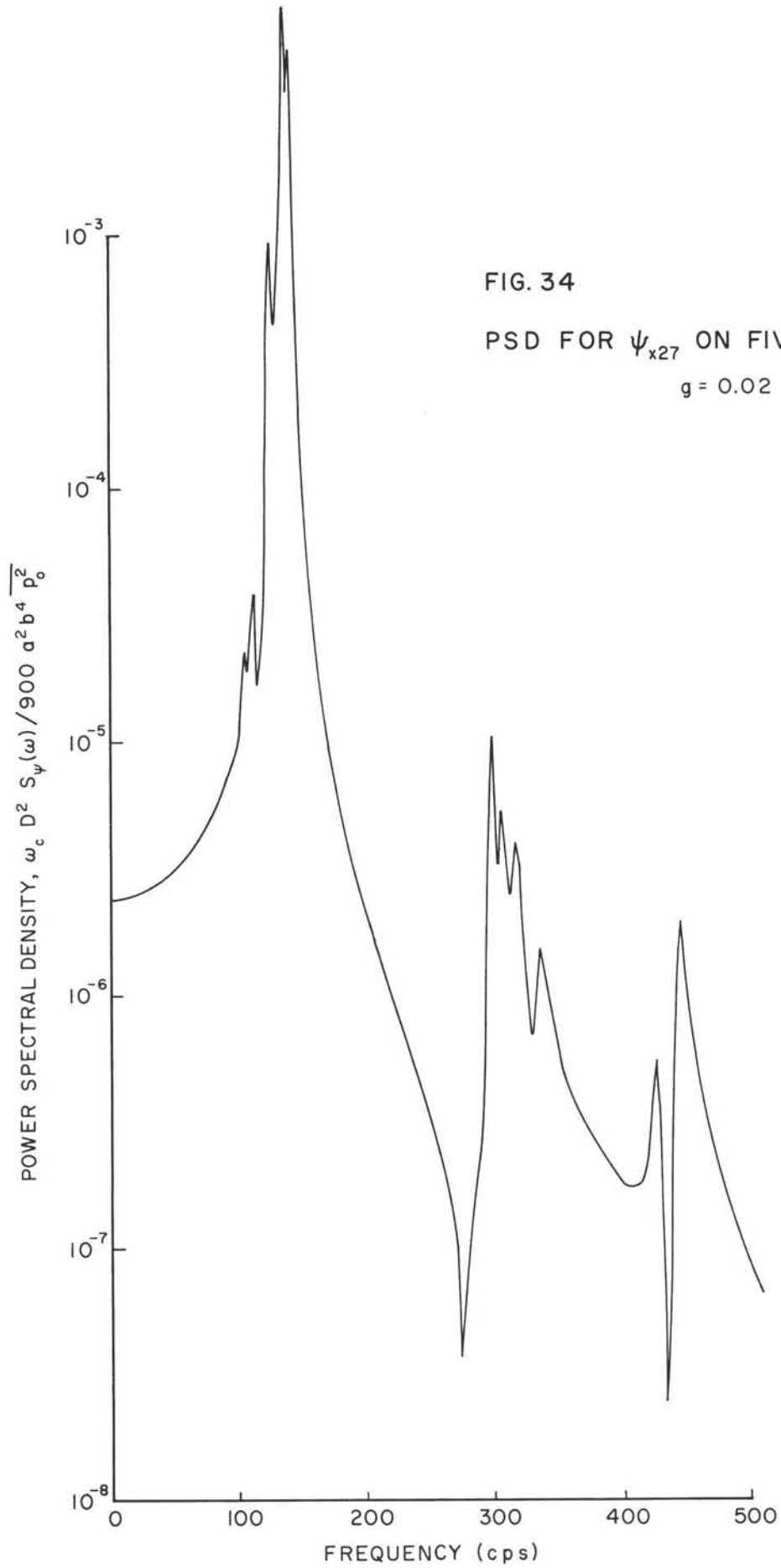
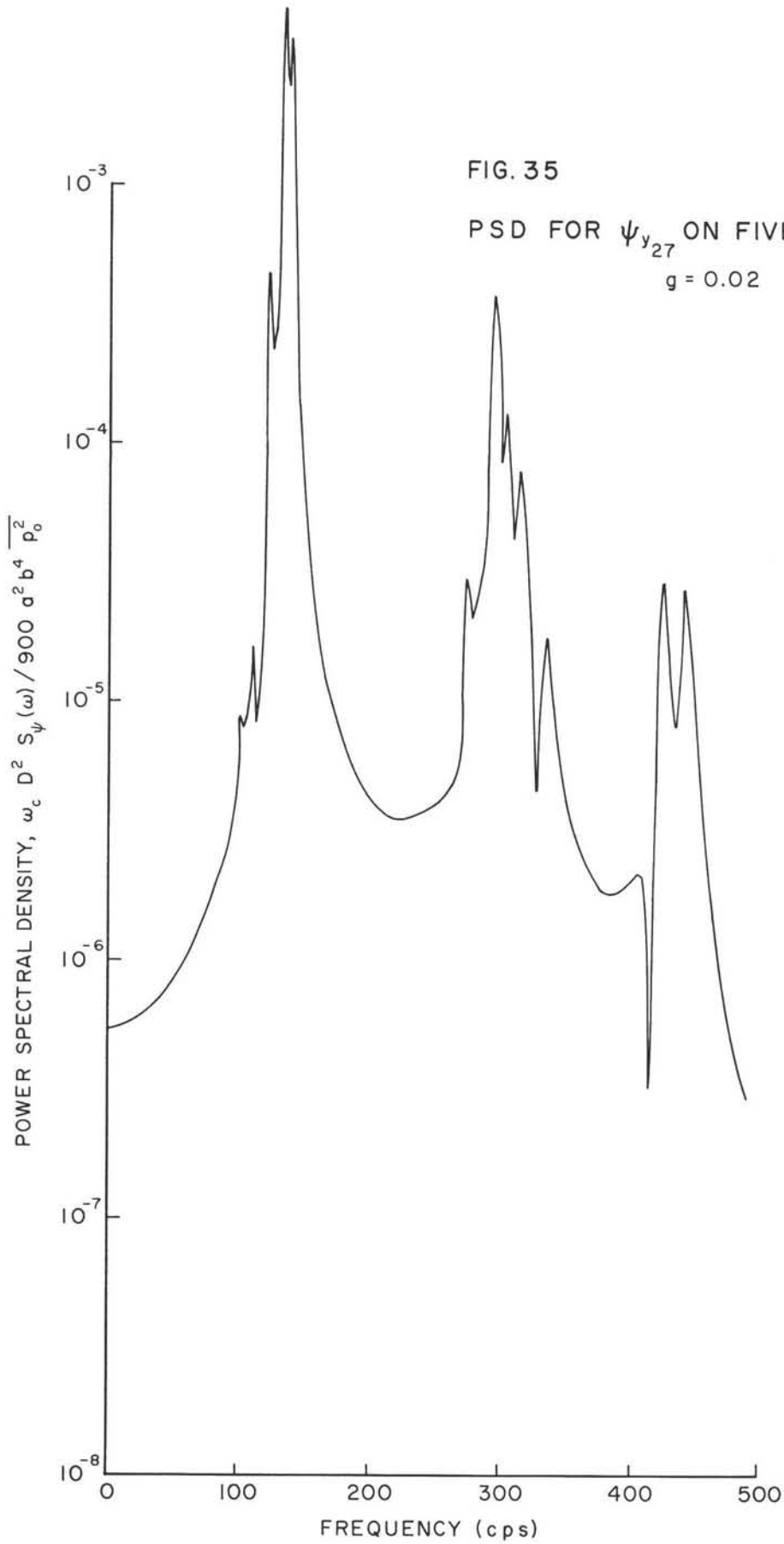


FIG. 34

PSD FOR ψ_{x27} ON FIVE-BAY PANEL
g = 0.02



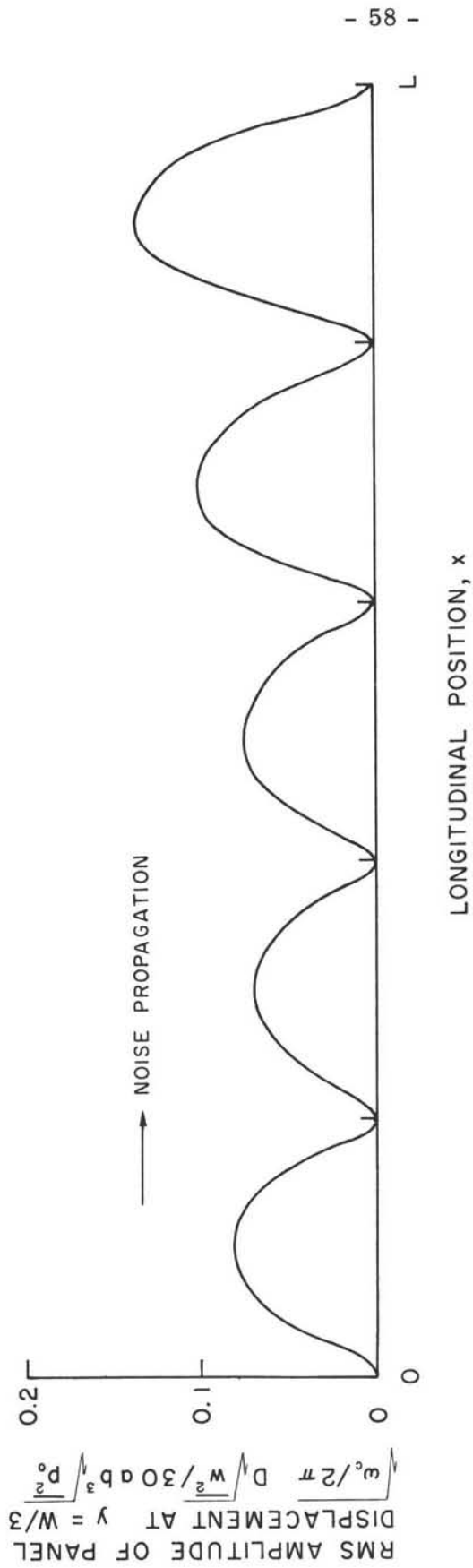


FIG. 36 LONGITUDINAL DISTRIBUTION OF RMS PANEL RESPONSE

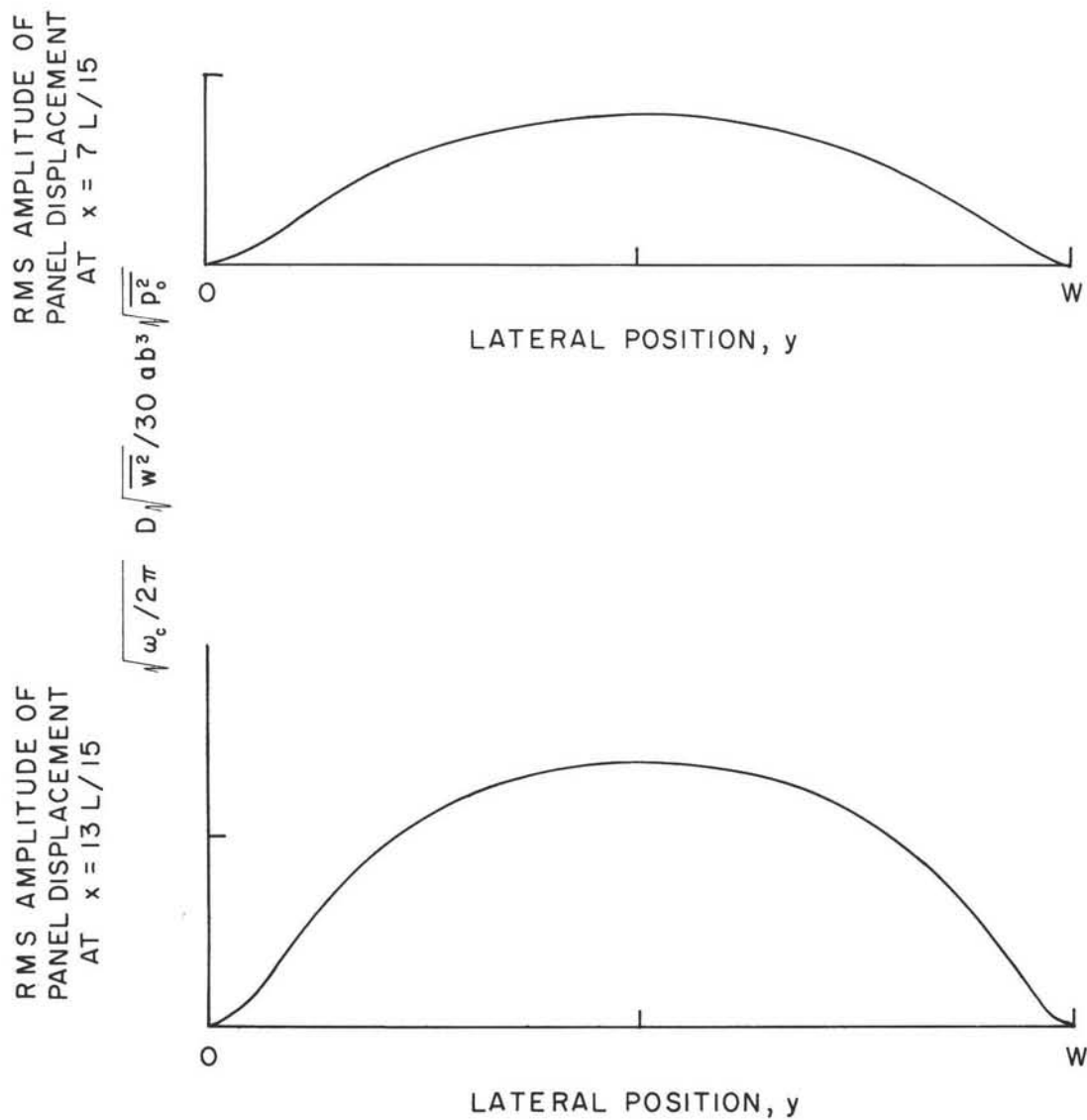
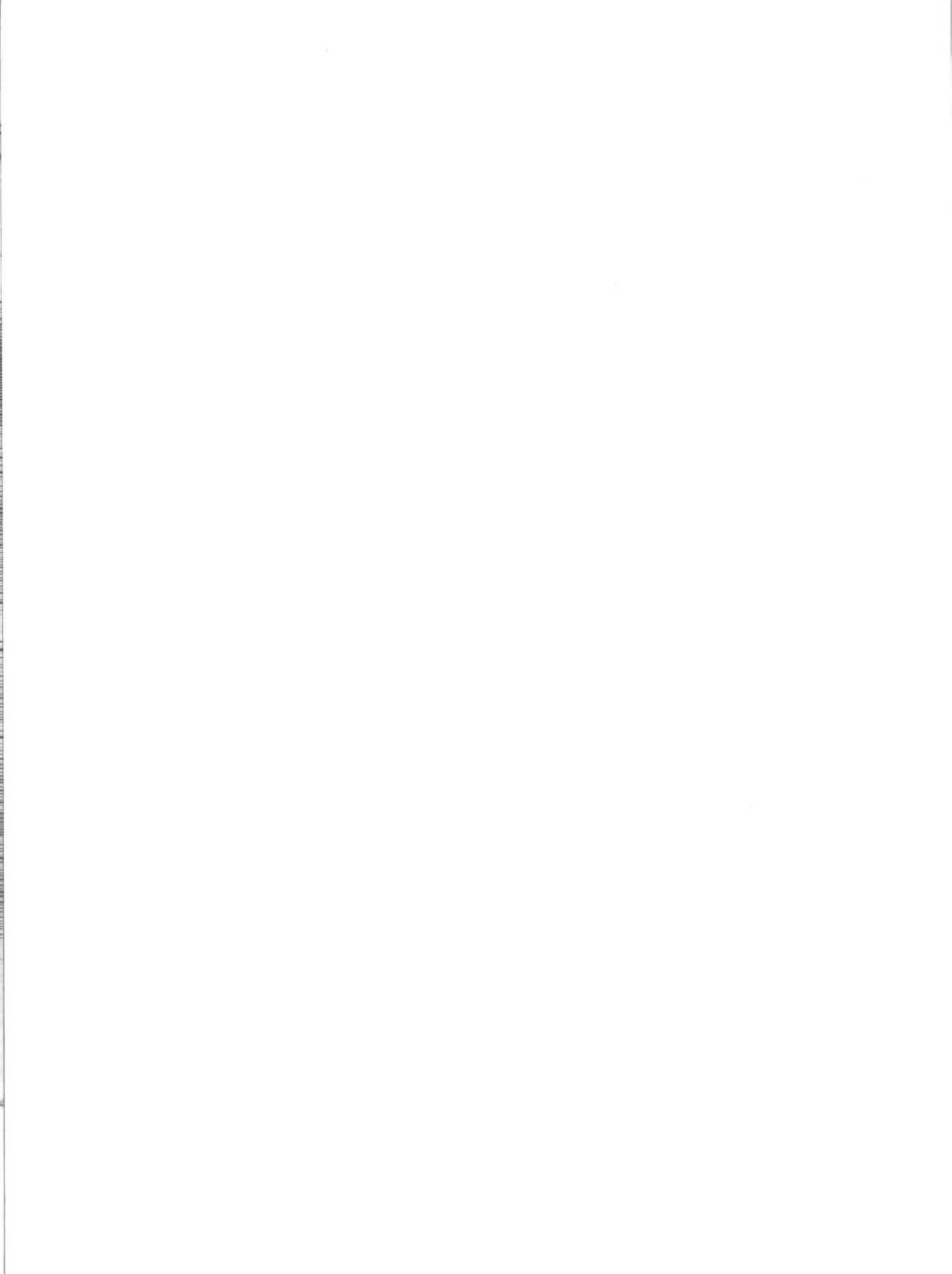


FIG. 37

LATERAL DISTRIBUTIONS OF RMS PANEL RESPONSE



APPENDIX A

DERIVATION OF STRINGER TORSIONAL ELEMENT

Assuming the rotation of the beam element shown in Figure 4 varies linearly in x , leads to the expression

$$\theta(x) = \left(1 - \frac{x}{\ell}\right) \theta_1 + \frac{x}{\ell} \theta_2 \quad (\text{A-1})$$

The strain energy for the beam element is

$$E_s = \frac{1}{2} \int_0^{\ell} GJ \left(\frac{d\theta}{dx}\right)^2 dx \quad (\text{A-2})$$

where GJ is the beam torsional rigidity, and the kinetic energy is

$$E_k = \frac{1}{2} \int_0^{\ell} I \left(\frac{d\theta}{dt}\right)^2 dx = \frac{\omega^2}{2} \int_0^{\ell} I \theta^2 dx \quad (\text{A-3})$$

for harmonic time dependence where I is the moment of inertia per unit length of beam.

Substituting the expression for $\theta(x)$ into the energy integrals and carrying out the integrations, yield

$$E_s = \frac{1}{2} X^T K X \quad (\text{A-4})$$

$$E_k = \frac{\omega^2}{2} X^T M X$$

where

$$X^T = [\theta_1, \theta_2]$$

and

$$K = \frac{GJ}{\ell} \begin{bmatrix} 1 & -1 \\ -1 & 1 \end{bmatrix}$$

and

$$M = \frac{I\ell}{6} \begin{bmatrix} 2 & 1 \\ 1 & 2 \end{bmatrix}$$

are the stiffness and mass matrices for the beam torsional element. Hence, the equation relating the end rotations θ_1 and θ_2 to the applied end torques T_1 and T_2 (Fig. 4) may be put in the form

$$\begin{bmatrix} T_1 \\ T_2 \end{bmatrix} = \frac{GJ}{\ell} \begin{bmatrix} 1 & -1 \\ -1 & 1 \end{bmatrix} \begin{bmatrix} \theta_1 \\ \theta_2 \end{bmatrix} - \frac{I\omega^2\ell}{6} \begin{bmatrix} 2 & 1 \\ 1 & 2 \end{bmatrix} \begin{bmatrix} \theta_1 \\ \theta_2 \end{bmatrix} \quad (\text{A-5})$$





